AJS American Journal of Science
publishing earth-sciences research since 1818

Bowyer, F., Yilales, M., Wood, R., & Poulton, S. W. (2023). Insights Into the Terminal Ediacaran Marine Carbonate Record From Shale-Hosted Carbonate Carbon Isotopes. *American Journal of Science*, *323*, 9. https://doi.org/10.2475/001c.88082

Science Paper

Insights Into the Terminal Ediacaran Marine Carbonate Record From Shale-Hosted Carbonate Carbon Isotopes

Fred Bowyer[1a], Mariana Yilales[1], Rachel Wood[1], Simon W. Poulton[2]

[1] School of GeoSciences, University of Edinburgh, [2] School of Earth and Environment, University of Leeds

Keywords: Ediacaran, carbon isotope, chemostratigraphy, organic carbon, diagenesis

https://doi.org/10.2475/001c.88082

American Journal of Science

Vol. 323, 2023

The marine carbon isotope record ($\delta^{13}C$) used for chemostratigraphy and reconstruction of carbon cycle dynamics is commonly assembled using carbonate rocks. There is, however, evidence that carbonate cements hosted within fine-grained clastics (shales and mudstones) in some settings may also express $\delta^{13}C$ trends that covary with the record from carbonates. We present new carbon and oxygen isotopic data from shale-hosted carbonate cements (herein termed $\delta^{13}C_{carb\text{-}sh}$ and $\delta^{18}O_{carb\text{-}sh,}$ n = 107, <16 wt% $CaCO_3$) of the terminal Ediacaran Nama Group, Namibia (⩾550.5 to <539.6 Million years ago; Ma). These data are compared with the published carbon and oxygen isotopic record from coeval carbonates ($\delta^{13}C_{carb}$ and $\delta^{18}O_{carb}$, n = 1611) and total organic carbon (TOC) concentrations. We show that, in the Nama Group, $\delta^{13}C_{carb\text{-}sh}$ compositions in samples of intermediate to high $CaCO_3$/TOC (>0.4) can approximate contemporaneous $\delta^{13}C_{carb}$ in open marine mixed carbonate-clastic settings. By contrast, $\delta^{13}C_{carb\text{-}sh}$ values in samples with low $CaCO_3$/TOC (<0.4) that were deposited in clastic settings distant from the locus of carbonate deposition are more negative than contemporaneous $\delta^{13}C_{carb}$. These data suggest that $\delta^{13}C_{carb\text{-}sh}$ may approach seawater composition in samples with low TOC when deposited in settings characterized by high CO_3^{2-} concentration, where carbonate can rapidly precipitate from seawater during early diagenesis. However, the use of $\delta^{13}C_{carb\text{-}sh}$ to infill gaps in the existing $\delta^{13}C_{carb}$ record remains uncertain, even when these criteria are fulfilled. Intervals of $\delta^{13}C$-$\delta^{18}O$ co-variability in the Nama Group succession appear to correlate with units where seawater mixing with meteoric fluids was more likely during early diagenesis, such as clastic-dominated settings, which also show significant decreasing $\delta^{18}O$ through time with gradual sub-basin infill. We further consider uncertainties in lithostratigraphic correlation of the upper Urusis Formation of the Nama Group that enable three new possible correlations to be proposed for $\delta^{13}C_{carb\text{-}sh}$ data within the terminal Ediacaran to lower Cambrian (<542.65 Ma to >532 Ma) regional and global $\delta^{13}C_{carb}$ records.

1. INTRODUCTION

The marine $\delta^{13}C$ curve is used to understand the evolution of the carbon cycle and for chemostratigraphic correlation through geological time (Cramer & Jarvis, 2020). Long-term changes in seawater $\delta^{13}C$ are often considered to reflect the net production, flux, burial, and oxidation of isotopically light organic matter (e.g., Veizer & Hoefs, 1976). However, local pools of DIC with distinct isotopic composition and sediment-buffered versus fluid-buffered diagenetic regimes may result in significant deviation of the carbon isotopic composition preserved by carbonate cements and sediments ($\delta^{13}C_{carb}$) from global average seawater $\delta^{13}C_{DIC}$ (Ahm & Husson, 2022; Cui et al., 2020; Geyman & Maloof, 2019; Hoffman & Lamothe, 2019; Melim et al., 2002). Notwithstanding these local effects, global composite $\delta^{13}C_{carb}$ records that are calibrated using available radiometric constraints in multiple regions throughout the late Neoproterozoic to early Phanerozoic appear to suggest that numerous $\delta^{13}C_{carb}$ excursions recorded within individual successions may be globally synchronous (e.g., Bowyer et al., 2022; Halverson et al., 2005; Maloof et al., 2010; Nelson et al., 2023; Yang et al., 2021). These excursions may therefore be driven by globally synchronous processes including, but not limited to, changes in the relative volumes of siliciclastic vs carbonate sedimentation, nutrient delivery, or eustatic sea level (Ahm et al., 2021).

a Corresponding author: fred.bowyer@ed.ac.uk

The $\delta^{13}C$ record is assembled using carbonate rocks or bioclasts, but clastic rocks (sandstones, siltstones, shales, or conglomerates) are commonly excluded because their authigenic carbonate cements are assumed to have precipitated later under burial diagenetic conditions, rather than from seawater. However, carbonate cements within some Neoproterozoic clastic rocks have also recently been shown to record trends in $\delta^{13}C$ that are radiometrically calibrated to be synchronous with global excursions in the $\delta^{13}C$ record derived from coeval carbonate rocks, albeit with some variable offsets (Canfield et al., 2020). This raises the possibility that $\delta^{13}C$ data derived from shale-hosted carbonate cements (herein termed $\delta^{13}C_{carb\text{-}sh}$ to aid distinction from $\delta^{13}C_{carb}$ of coeval carbonates), in some depositional and diagenetic settings, may be useful to establish stratigraphic correlations and to infer carbon cycle behavior in otherwise poorly constrained clastic successions. A crucial pre-requisite for the application of $\delta^{13}C_{carb\text{-}sh}$ for chemostratigraphy is to understand the mechanisms for, and extent of, $\delta^{13}C_{carb\text{-}sh}$ deviation from regional $\delta^{13}C_{carb}$ records.

The isotopic composition of a carbonate mineral is dependent upon the composition of the solution from which it precipitates, and the effects of post-depositional diagenetic alteration (e.g., Ahm et al., 2018; Swart, 2015). The oxygen isotopic composition ($\delta^{18}O$) of inorganic carbonates is largely dependent upon the $\delta^{18}O$ composition of the precipitating fluid, the temperature of precipitation, and the resulting carbonate mineralogy (e.g., Epstein et al., 1953; Epstein & Mayeda, 1953; Tarutani et al., 1969; Urey, 1947). Seawater is generally enriched in ^{18}O relative to freshwater, and carbonate precipitates that are altered within the meteoric mixing zone therefore commonly show positive covariation between $\delta^{13}C$ and $\delta^{18}O$ that reflects these two end-member solution compositions (Allan & Matthews, 1982; Swart, 2015). Lower values of $\delta^{18}O$ are also associated with higher burial temperatures (Urey, 1947), and co-variation between $\delta^{13}C$ and $\delta^{18}O$ may therefore also occur as a consequence of mixing between low temperature, fluid-buffered carbonates and high temperature, sediment-buffered carbonates (Ahm et al., 2018).

Here we present new $\delta^{13}C_{carb\text{-}sh}$ data from the fossiliferous terminal Ediacaran Nama Group, Namibia (⩾550.5 Ma to <539.6 Ma). The succession comprises mixed carbonates and clastics with well-established intra- and inter-basinal correlations and abundant dated ash beds, but the regional composite $\delta^{13}C_{carb}$ curve is discontinuous (Bowyer et al., 2022; Germs, 1983; Germs & Gresse, 1991; Linnemann et al., 2019; Nelson et al., 2022; Saylor et al., 1998; Wood et al., 2015). A proposed chemostratigraphic marker for the Ediacaran-Cambrian boundary corresponds to the stratigraphic position of a large magnitude negative $\delta^{13}C_{carb}$ excursion, termed the '1n/BACE' (min. $\delta^{13}C_{carb}$ = ~-10‰), relative to key fossil occurrences, including the first appearance datum (FAD) of the ichnospecies *Treptichnus pedum* (Brasier et al., 1994; Zhu et al., 2006). Whilst recent radiometric ages from Laurentia constrain recovery from the 1n/BACE at ca. ⩽533 Ma (Nelson et al., 2023), numerous uncertainties remain in the precise age of the 1n/BACE onset (reviewed in Bowyer et al., 2022), and the sequence of regional and global biotic first appearances across the 1n/BACE (e.g., Bowyer, Zhuravlev, et al., 2023; Topper et al., 2022). The 1n/BACE has been recorded in multiple successions globally (e.g., Bowyer, Uahengo, et al., 2023; Hodgin et al., 2021; Kouchinsky et al., 2007; Maloof et al., 2010; E. F. Smith, Nelson, et al., 2016; Topper et al., 2022; Zhu et al., 2019), but is notably absent from the Nama Group (Nelson et al., 2022; Saylor et al., 1998; Wood et al., 2015). This may suggest that the onset of this excursion is younger than *ca.* 538 Ma, and therefore postdates carbonate sedimentation in the Nama Group succession (Bowyer et al., 2022; Bowyer, Zhuravlev, et al., 2023; Nelson et al., 2022, 2023) (but see discussion).

We assess the potential for siliciclastic rocks to record $\delta^{13}C$ values that approximate seawater composition throughout deposition of the Nama Group. First, measurements of $\delta^{13}C_{carb\text{-}sh}$ are compared with the magnitudes and trends in $\delta^{13}C_{carb}$ recorded by carbonate interbeds and laterally correlative carbonate-clastic successions. We then interrogate stratigraphic intervals that show covariation between $\delta^{13}C$ and $\delta^{18}O$, using published carbonate data and new clastic data, to identify possible alteration of $\delta^{13}C$ from seawater composition associated with meteoric diagenesis. Covariation between $\delta^{13}C_{carb\text{-}sh}$ and the concentrations of calcium carbonate ($CaCO_3$) and total organic carbon (TOC) are also evaluated in order to explore the potential for differences in bulk shale composition to result in deviation of $\delta^{13}C_{carb\text{-}sh}$ from $\delta^{13}C_{carb}$. Lastly, we explore the chemostratigraphic alignment of new $\delta^{13}C_{carb\text{-}sh}$ data within alternative lithostratigraphic correlations for the Urusis Formation of the Nama Group (⩽543 to ⩽538.6 Ma) and consider the utility of the $\delta^{13}C_{carb\text{-}sh}$ data to infill gaps in the composite regional $\delta^{13}C$ curve across the critical ⩾550.5 to <538 Ma interval. We compare the composite $\delta^{13}C$ record for the upper Nama Group with regional composite $\delta^{13}C$ records from other approximately-contemporaneous successions deposited across the terminal Ediacaran to lowermost Cambrian interval, in order to evaluate the inter-regional consistency of magnitudes and trends in $\delta^{13}C$ and the implications for calibrated global biostratigraphy.

2. GEOLOGICAL SETTING OF THE NAMA GROUP

The Nama Group in southern Namibia (⩾550.5 to <538 Ma) is a mixed carbonate and siliciclastic foreland basin succession deposited in supratidal to outer ramp settings in the Zaris and Witputs sub-basins (fig. 1A; Germs, 1983; Gresse & Germs, 1993). Sediments within the Zaris and Witputs sub-basins were deposited during cratonic convergence along the Damara and Gariep orogenies, to the north and southwest, respectively (Germs, 1983; Germs & Gresse, 1991; Gresse & Germs, 1993). Strata within both sub-basins have been correlated using litho- and chemostratigraphy, and correlation of stratal stacking patterns have informed sequence stratigraphy (figs. 1 and 2; e.g., Bowyer, Uahengo, et al., 2023; Germs, 1983; Nelson et al., 2022; Saylor et al., 1995, 1998; Wood et al., 2015). Intervals of the Nama Group succession have also been accurately age-calibrated via U-Pb zircon geochronology of interbedded tuff deposits (fig. 2; Bowring et al., 2007; Grotzinger et al., 1995; Linnemann

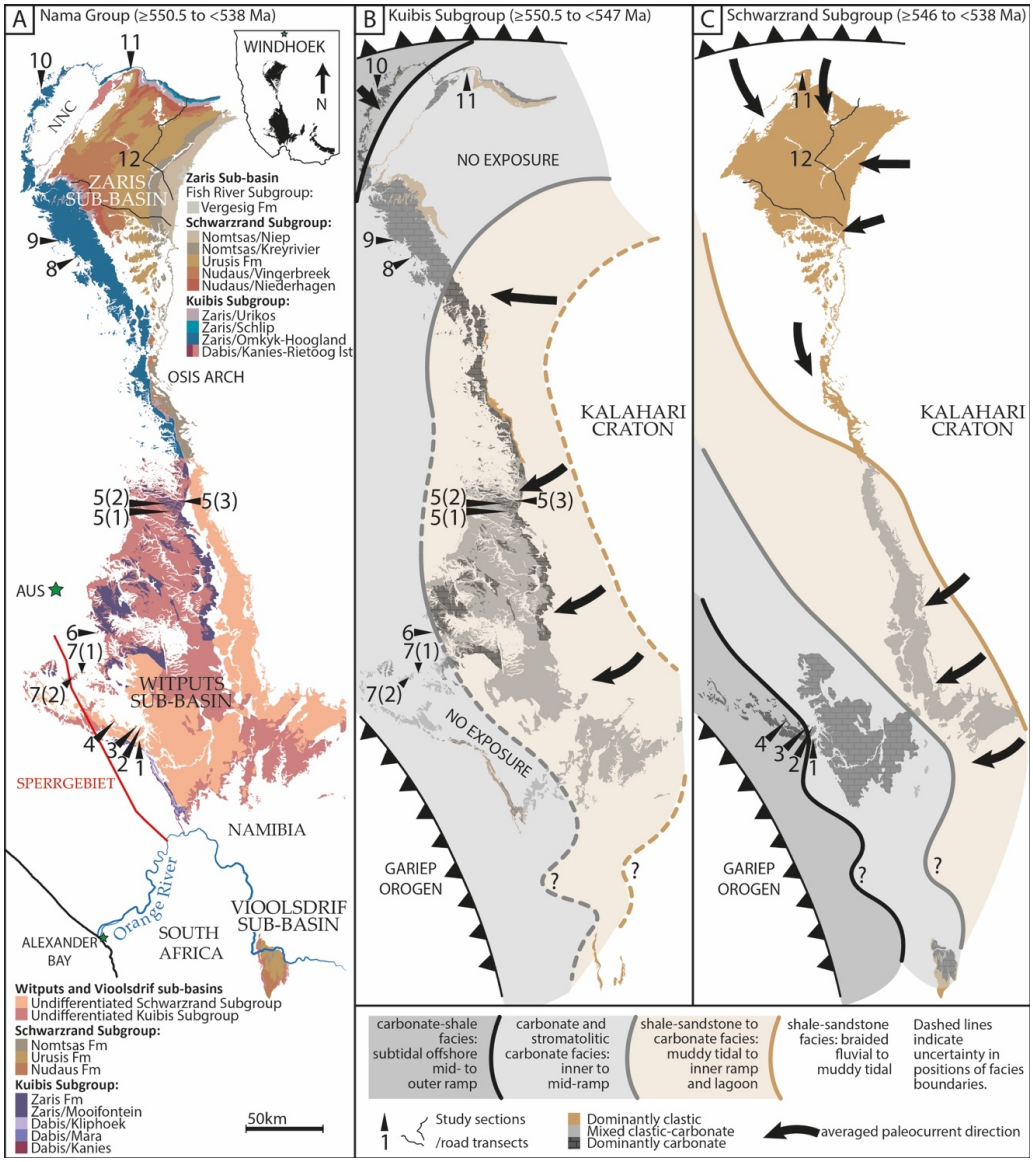

Figure 1.

(A) Geological map of the Nama Group with pins showing precise positions of sections discussed in the text. Map drafted using 1:250000 maps of Ai-Ais (Sheet 2716, 2010), Bethanien (Sheet 2616, 1999), Gibeon (Sheet 2516, 2000), Mariental (Sheet 2416, 2017), and Rehoboth (Sheet 2316, 2006), Geological Survey of Namibia, Ministry of Mines and Energy, and map of Neint Nababeep Plateau after Nelson et al. (2022) and references therein. (B) Dominant lithology, interpreted facies and average paleocurrent directions for outcrop of the Kuibis Subgroup (≥550.5 to <547 Ma; after Germs, 1983). (C) Dominant lithology, interpreted facies, and average paleocurrent directions for outcrop of the Schwarzrand Subgroup (≥546 to <538 Ma; after Germs, 1983).

et al., 2019; Nelson et al., 2022). The age of the base of the Nama Group remains uncertain but is estimated to be ⩾550.5 Ma (Bowyer et al., 2022; Saylor et al., 1998), and the youngest dated tuff deposit in the Witputs Sub-basin, immediately overlying the sub-Nomtsas Formation unconformity, yields a U-Pb age of 538.58 ± 0.19 Ma (Linnemann et al., 2019).

The succession is divided into the lower Nama Group (Kuibis Subgroup, *ca.* ⩾550.5 to <547 Ma), and upper Nama Group (Schwarzrand Subgroup, *ca.* ⩾546 to <538 Ma; fig. 1). A mixed carbonate-siliciclastic succession deposited in the Vioolsdrif Sub-basin of northwest South Africa is radiometrically constrained to be temporally equivalent to, at minimum, the Schwarzrand Subgroup of the Witputs Sub-basin (Nelson et al., 2022). The Witputs and Vioolsdrif sub-basins may have been separated by a tectonic forebulge (the Koedoelaagte Arch; Germs & Gresse, 1991).

The Zaris and Witputs sub-basins deepened to the (present-day) north and southwest, respectively, during deposition of the Kuibis Subgroup, with increasing distance from an intervening paleobathymetric high (the Osis Arch), and with distance from the Kalahari Craton to the present east (fig. 1B; Germs, 1983). However, gradual infill of the Zaris Sub-basin shifted the orientation of facies belts to northwest-southeast across both sub-basins during deposition of the Schwarzrand Subgroup (fig. 1C; Germs, 1983; Saylor, 2003; Saylor et al., 1995). Facies belts range from clastic-dominated braided-fluvial to muddy tidal, to inner, mid- and finally outer ramp carbonate-dominated facies, which deepened, on average, to the west or south-west during deposition of the Schwarzrand Subgroup (Germs, 1983; Say-

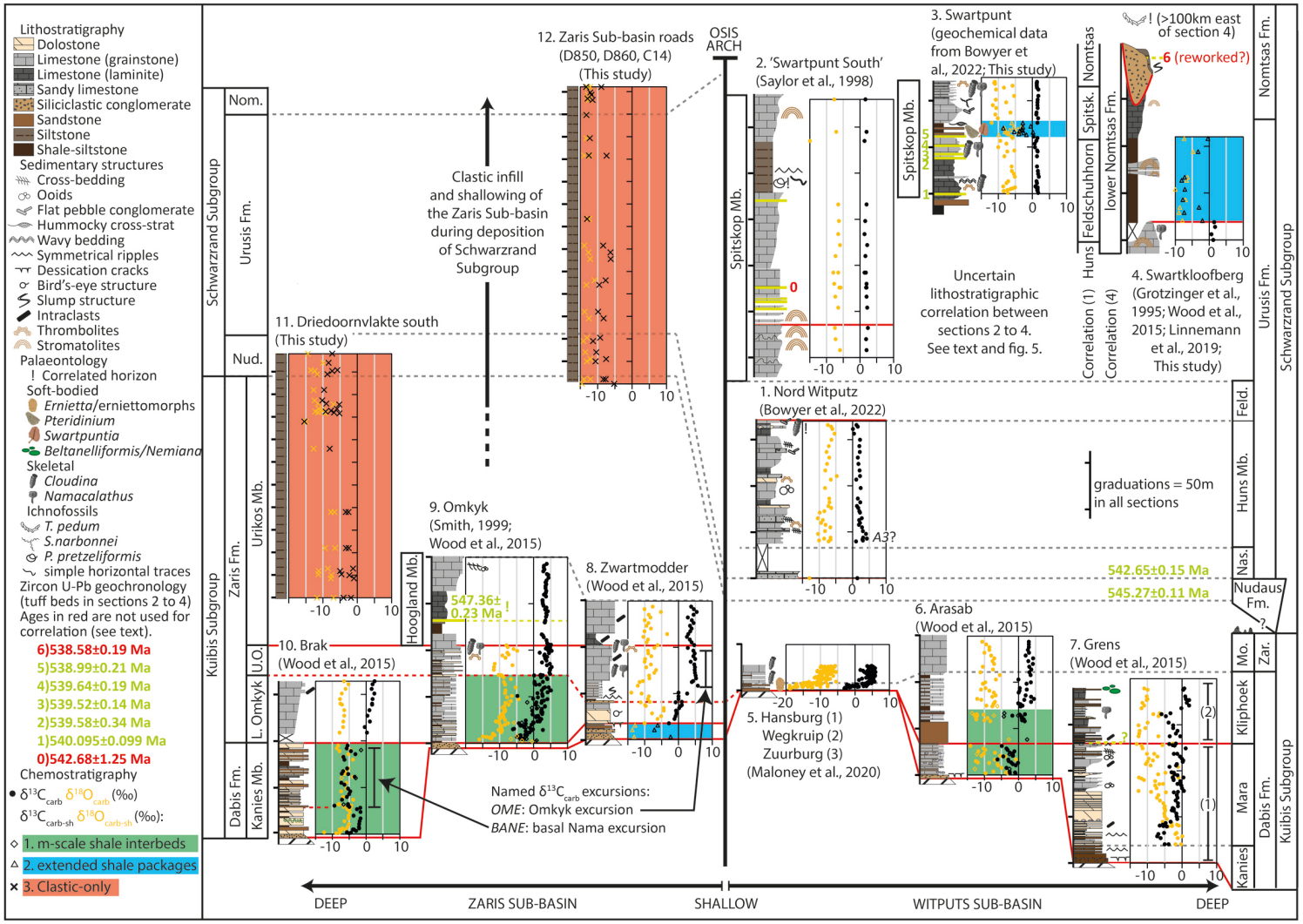

Figure 2. Lithostratigraphy and chemostratigraphy of sections discussed in the text, including those sampled for $\delta^{13}C_{carb\text{-}sh}$ (subdivided into groups 1 to 3), with additional published $\delta^{13}C_{carb}$ data after Saylor et al. (1998), Smith (1999), Wood et al. (2015), Maloney et al. (2020), and Bowyer et al. (2022).

Dated ash beds after Grotzinger et al. (1995, recalculated in Schmitz, 2012), Bowring et al. (2007), Linnemann et al. (2019), and Nelson et al. (2022). U.O. = Upper Omkyk Mb, Nud. = Nudaus Fm, Nom. = Nomtsas Fm, Mo. = Mooifontein Mb, Zar. = Zaris Fm, Nas. = Nasep Mb, Feld. = Feldschuhhorn Mb, Spitsk. = Spitskop Mb. Alternative correlations for sections 1 to 4, including correlations (1) and (4) shown for section 4, are discussed further in the text and figs. 5 to 7.

lor, 2003). The Kalahari craton was the main source of clastic sediment into the Nama sub-basins during deposition of the Kuibis Subgroup (fig. 1B; Germs, 1983), but during deposition of the Schwarzrand Subgroup, the Zaris Sub-basin received additional detrital material directly from the Damara Belt to the north (fig. 1C; Blanco et al., 2009, 2011; Germs, 1983). In the Nama Group successions, early Transgressive Systems Tracts are generally dominated by siliciclastic rocks whereas various carbonate facies distinguish late Transgressive to Highstand Systems Tracts (Saylor et al., 1995, 1998).

3. METHODS

$\delta^{13}C_{carb\text{-}sh}$ and $\delta^{18}O_{carb\text{-}sh}$ data were obtained from 107 shale/mudstone samples (defined as <16 wt% $CaCO_3$) collected from eight outcrop sections distributed across both the Zaris and Witputs sub-basins, which together cover ⩾12 Myr from the Kanies Member of the Dabis Formation (⩾550.5 Ma) to the Nomtsas Formation (⩽538.6 Ma; fig. 2, table S1). Samples were taken from three settings: (1) three sections of the lower Kuibis Subgroup that contain intervals composed of decimeter to meter-scale interbedded carbonates and clastics (⩽1 m) deposited on the inner to mid-outer ramp (n = 21, sections 6, 9 and 10; figs. 1B, 2, 3A,B); (2) three extended shale packages (12–90 m) within carbonate-clastic successions, one from a shallow-inner ramp section of the Kuibis Subgroup (n = 3, section 8; figs. 1B and 2), and two from the Schwarzrand Subgroup deposited on the mid- to outer ramp (n = 21, sections 3 and 4; figs. 1C, 2, 3C–E); (3) two composite sampling transects through clastic-only successions of the uppermost Kuibis Subgroup and entire Schwarzrand Subgroup (n = 62, sections 11 and 12; figs. 1B and C, 2, 3F,G) that record an overall shallowing-upward succession from mid-ramp to inner ramp and lagoon. Samples from these three settings are classified into three groups: Group 1: m-scale shale interbeds within carbonate-clastic successions; Group 2: extended shale packages within carbonate-clastic successions, and Group 3: clastic-only successions.

Analyses of $\delta^{13}C_{carb\text{-}sh}$ followed the method of Canfield et al. (2020). Powdered bulk clastic rock samples in sealed vials were reacted with 100% orthophosphoric acid at 75 °C and left for 24 h using an Elementar iso FLOW system. Any resulting CO_2 gas produced was then extracted from the vial and analyzed for its carbon and oxygen isotopic ratios using an Elementar PRECISION stable isotope ratio mass spectrometer. The standard deviation (n = 48) of a powdered coral laboratory standard (COR1D, $\delta^{13}C$ = -0.649‰, $\delta^{18}O$ = -4.924‰) run as a sample on the same days as the study samples, was ± 0.074‰ for $\delta^{13}C_{carb}$ and ± 0.111‰ for $\delta^{18}O_{carb}$. All isotopic values are normalized relative to the Vienna Pee Dee Belemnite (VPDB) standard. Total wt% $CaCO_3$ in shales was estimated using a linear regression model between peak height area from the isotopic measurements and the analyzed mass of powdered coral laboratory standard (COR1D, assumed 100% $CaCO_3$). The uncertainty associated with this regression model is <1% (see Supplementary Information). A subset of shale samples of varying $CaCO_3$ concentration from different sections were also analyzed by colorimeter, and the relative concentrations of $CaCO_3$ were consistent between both methods (table S2). We also consider published TOC concentration data from the same samples analyzed herein for $\delta^{13}C_{carb\text{-}sh}$ (Bowyer et al., 2020).

$\delta^{13}C_{carb\text{-}sh}$ data (n = 107) were compared to available $\delta^{13}C_{carb}$ from 38 sections (n = 1611) of the Nama Group succession in Namibia and northwest South Africa. In order to test the degree to which these data may reflect early diagenetic resetting from seawater $\delta^{13}C$ composition associated with mixing between two end-member compositions, we assessed the co-variation of $\delta^{13}C$ and $\delta^{18}O$. In order to test whether values of $\delta^{13}C_{carb\text{-}sh}$ are affected by the concentrations of $CaCO_3$ or TOC within each sample, we tested the co-variation of $\delta^{13}C_{carb\text{-}sh}$ and $CaCO_3$, and $\delta^{13}C_{carb\text{-}sh}$ and TOC. In each case, the Shapiro-Wilk test was used to evaluate whether these data are normally distributed (tables S3 and S4). The strength and significance of correlations were tested using either Pearson's correlation coefficient (r), or the non-parametric equivalent test of Spearman's rank correlation coefficient (ρ). Spearman's rank correlation coefficient was used when assumptions about the normality of the distribution of the variables, constant residual variability, and linearity were not fulfilled. In each case, significant correlations are indicated when $p \leqslant 0.05$.

Lastly, we explore the alternative regional $\delta^{13}C$ chemostratigraphies that result from different possible lithostratigraphic correlations between sections of the Urusis Formation within the Witputs Sub-basin and between the Witputs and Vioolsdrif sub-basins. All new and existing data are calibrated with available radiometric dates and placed within the resulting composite Nama Group $\delta^{13}C$ chemostratigraphic age frameworks (updated from Bowyer et al., 2022 and Bowyer, Zhuravlev, et al., 2023).

4. RESULTS

4.1. Group 1: Meter-scale shale interbeds within carbonate-clastic successions

The $\delta^{13}C_{carb\text{-}sh}$ data for m-scale shale interbeds within carbonate-clastic successions range from -6.63‰ to +2.50‰ (mean = -1.62‰, sd = 2.38‰, n = 21, table S1). Through the Dabis Formation and lower Zaris Formation (⩾550.5 to *ca.* 547 Ma), $\delta^{13}C_{carb\text{-}sh}$ values from Arasab, Omkyk and Brak (sections 6, 9, 10, fig. 2) closely follow the negative-to-positive trend recorded by contemporaneous $\delta^{13}C_{carb}$ (fig. 2).

$\delta^{13}C_{carb\text{-}sh}$ values do not show a statistically significant correlation with $\delta^{18}O_{carb\text{-}sh}$ ($r = 0.42$, $p = 0.06$, $R^2 = 0.17$, fig. 4A). These interbedded shales are characterized by $CaCO_3$ concentrations in the range 0.02–15.51 wt% (mean = 2.42 wt%, fig. 4B), TOC concentrations in the range 0.04–0.11 wt% (mean = 0.07 wt%, fig. 4C), and $CaCO_3$/TOC in the range 0.4–85.0 (mean = 11.83, fig. 4D). There is no significant correlation between $\delta^{13}C_{carb\text{-}sh}$ and $CaCO_3$ content ($\rho = 0.07$, $p = 0.77$, fig. 4B), $\delta^{13}C_{carb\text{-}sh}$ and TOC content ($\rho = -0.49$, $p = 0.15$, fig. 4C), or $\delta^{13}C_{carb\text{-}sh}$ and $CaCO_3$/TOC ($\rho = -0.32$, $p = 0.37$, fig. 4D).

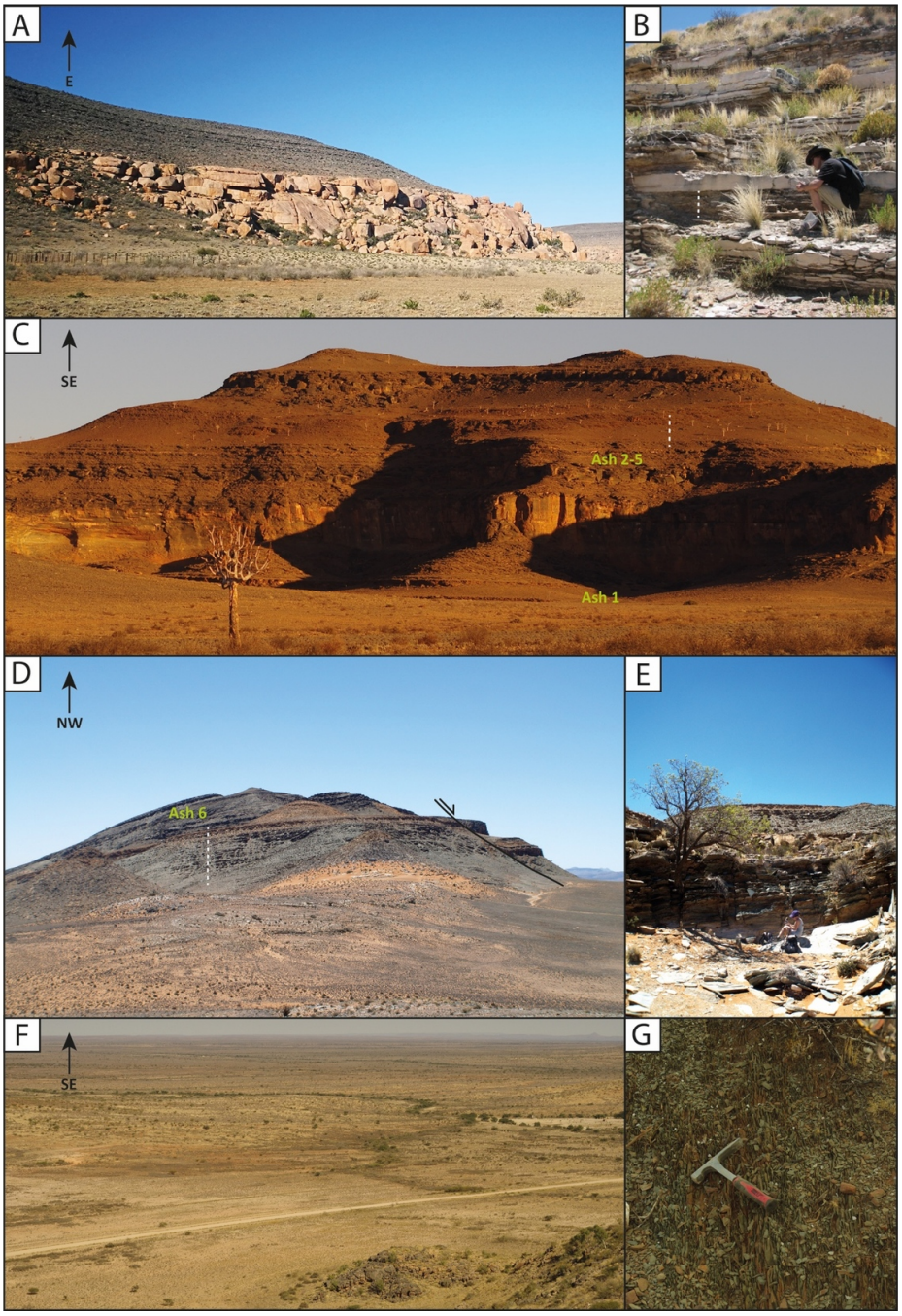

Figure 3. Outcrop photographs of selected study sections (fig. 2) and associated siliciclastic intervals.

(A) Nonconformable contact between the Mesoproterozoic Kobos granite and overlying mixed carbonate-siliciclastic sedimentary rocks of the lower Kuibis Subgroup at Farm Omkyk (section 9). (B) Group 1 samples. Decimeter to meter-scale shale interbeds in the mixed carbonate-clastic succession of the lower Omkyk Member (Zaris Formation) on Farm Omkyk (section 9). (C) Group 2 samples. Swartpunt (section 3) showing position of dated ash beds. Vertical dotted line demarks sampled shale interval. (D) Group 2 samples. Photograph showing position of extended shale package (vertical dotted line) sampled on Farm Swartkloofberg (section 4). Meter-sized fragments of ash bed 6 (Linnemann et al., 2019) occur above an erosional surface stratigraphically above the sampled interval (fig. 2). Normal fault recognized by Saylor and Grotzinger (1996) is noted in the right of the image. (E) Group 2 samples. Base of sampled siliciclastic interval on Farm Swartkloofberg (section 4). (F) Group 3 samples. Planate clastic succession constituting the Urikos Member of the Zaris Formation (foreground) shallowing up through the successions to the Nomtsas Formation (horizon), with increasing distance to the southeast. Photograph taken looking southeast from the Upper Omkyk Member at Farm Driedoornvlakte (section 11). (G) Group 3 samples. Example of shale-siltstone exposure from the clastic succession of the Schwarzrand Subgroup, Zaris Sub-basin. Digging was required to retrieve fresh material at each site.

4.2. Group 2: Extended shale packages within carbonate-clastic successions

Values of $\delta^{13}C_{carb\text{-}sh}$ from a 12.5 m-thick shale package of the Dabis Formation (Kuibis Subgroup, *ca.* 550.5 Ma) at Zwartmodder (section 8, fig. 2) range from -7.18‰ to -2.38‰ (n = 3). This interval records siliciclastic deposition during initial transgression across the Kalahari basement and has been litho- and chemostratigraphically correlated with transgressive limestone, dolostone and shale of the basal Omkyk Member at Omkyk (section 9), and the dolostone-dominated Dabis Formation at Brak (sections 10, fig. 2; Wood et al., 2015). $\delta^{13}C_{carb\text{-}sh}$ data at Zwartmodder overlap in magnitude and trend with both $\delta^{13}C_{carb\text{-}sh}$ and

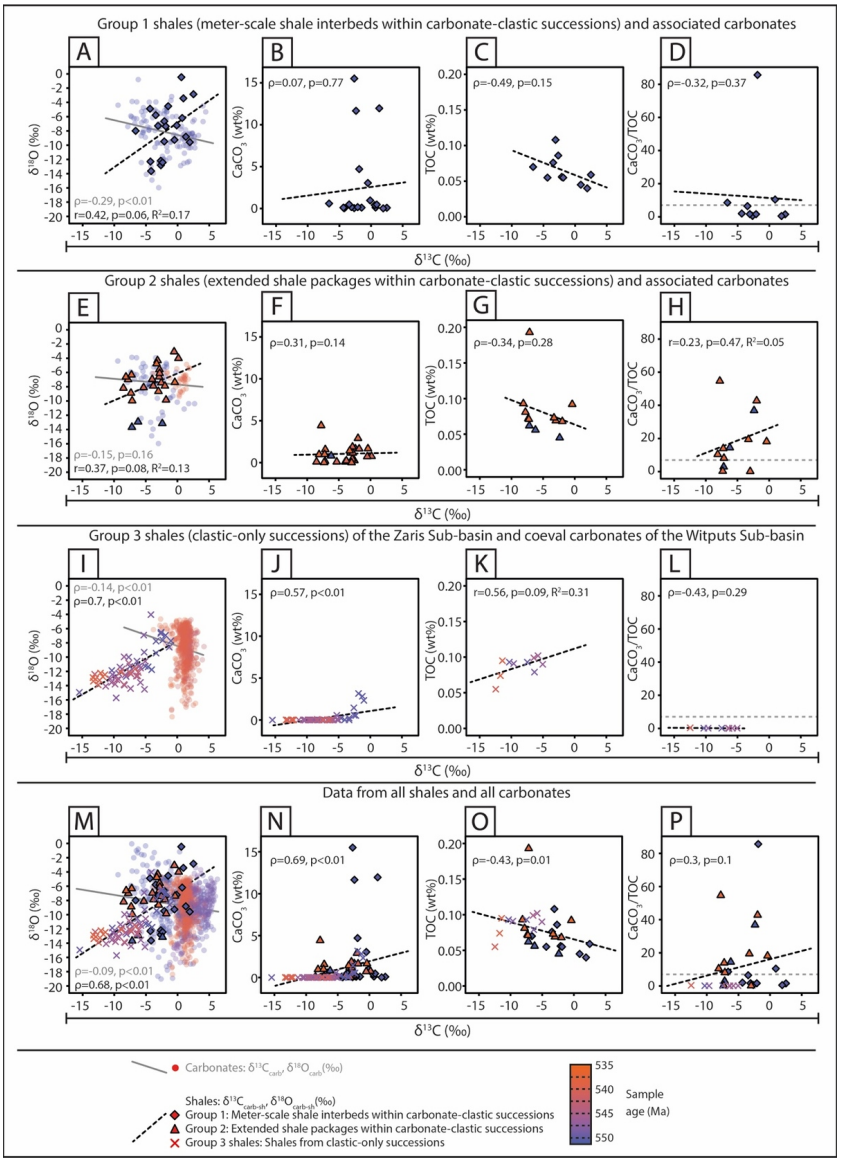

Figure 4.

(A), (E), (I), (M): $\delta^{18}O$ versus $\delta^{13}C$ for Group 1 shales and associated interbedded carbonates (A), Group 2 shales and associated carbonates (E), Group 3 shales and contemporaneous carbonates of the Witputs Sub-basin (I), and all studied shales and carbonates (M). Solid grey trend lines and statistical data are for carbonate samples, whereas dashed black trend lines and statistical data are for shale samples. (B), (F), (J), (N): $CaCO_3$ content versus $\delta^{13}C_{carb\text{-}sh}$ for Group 1 shales (B), Group 2 shales (F), Group 3 shales (J), and all studied shales (N). (C), (G), (K), (O): TOC versus $\delta^{13}C_{carb\text{-}sh}$ for Group 1 shales (C), Group 2 shales (G), Group 3 shales (K), and all studied shales (O). (D), (H), (L), (P): $CaCO_3$/TOC versus $\delta^{13}C_{carb\text{-}sh}$ for Group 1 shales (D), Group 2 shales (H), Group 3 shales (L), and all studied shales (P). Horizontal dashed lines in (D), (H), (L), and (P) mark the 7:1 threshold ratio of $CaCO_3$/TOC (after Saltzman & Thomas, 2012). Note that the x-axis of all panels corresponds to $\delta^{13}C$. All data symbols are colored according to approximate age, based on chemostratigraphic age model of Bowyer et al. (2022) updated with lithostratigraphic observations herein.

$\delta^{13}C_{carb}$ at Omkyk and Brak throughout this interval (figs. 2 and 4E).

$\delta^{13}C_{carb\text{-}sh}$ data from extended shale packages of the Urusis Formation (≤543 to ≤538.6 Ma), comprising the Swartpunt (section 3) and Swartkloofberg (section 4) sections, show dominantly negative values that range from -8.52‰ to +0.17‰ (mean = -4.01‰, sd = 2.69, n = 21, figs. 2 and 4E). $\delta^{13}C_{carb\text{-}sh}$ values at section 3 (-8.52‰ to +0.17‰, mean = -3.16‰, sd = 2.24, n = 12) appear scattered and depleted relative to $\delta^{13}C_{carb}$ above and below the siliciclastic interval (0.33–1.84‰, mean = 1.32‰, n = 36). However, $\delta^{13}C_{carb\text{-}sh}$ values at section 4 (-8.12‰ to -0.40‰, mean = -5.14‰, sd = 2.95, n = 9) broadly display both a falling limb from $\delta^{13}C_{carb}$ values recorded by underlying pinnacle reef carbonate (0.63–1.72‰, mean = 1.24, n = 4), followed by a nadir and a rising limb, which together appear to track the overall shape of a negative $\delta^{13}C_{carb\text{-}sh}$ excursion (fig. 2).

Group 2 shales do not show a statistically significant correlation between $\delta^{13}C_{carb\text{-}sh}$ and $\delta^{18}O_{carb\text{-}sh}$ ($r = 0.37$, $p = 0.08$, $R^2 = 0.13$; fig. 4E). These shale packages have $CaCO_3$ concentrations in the range 0.01–4.43 wt% (mean = 1.05 wt%, fig. 4F), TOC concentrations in the range 0.05–0.19 wt% (mean = 0.08 wt%, fig. 4G), and $CaCO_3$/TOC in the range 0.1–54.8 (mean = 18.49, fig. 4H). There is no statistically significant correlation between $\delta^{13}C_{carb\text{-}sh}$ and $CaCO_3$ content ($\rho = 0.31$, $p = 0.14$, fig. 4F), $\delta^{13}C_{carb\text{-}sh}$ and TOC

content (ρ = -0.34, p = 0.28, fig. 4G), or $\delta^{13}C_{carb\text{-}sh}$ and $CaCO_3$/TOC (r = 0.23, p = 0.47, R^2 = 0.05, fig. 4H).

4.3. Group 3: Clastic-only successions

$\delta^{13}C_{carb\text{-}sh}$ data from one clastic-only succession of the Urikos Member and Nudaus Formation of the Zaris Sub-basin (section 11, fig. 2), and a second composite clastic-only succession of the Urikos Member, and Nudaus, Urusis and Nomtsas formations of the Zaris Sub-basin (section 12, fig. 2), range from -15.45‰ to -1.00‰ (mean = -7.72‰, sd = 3.31, n = 62). These data are significantly depleted relative to $\delta^{13}C$ values of contemporaneous carbonates and shales from carbonate-clastic successions of the Zaris and Witputs sub-basins (figs. 2, 4I), and show a strong and statistically significant positive correlation between $\delta^{13}C_{carb\text{-}sh}$ and $\delta^{18}O_{carb\text{-}sh}$ (ρ = 0.70, p < 0.01, fig. 4I). This positive correlation also appears to be associated with the temporal distribution of samples, whereby values of $\delta^{13}C_{carb\text{-}sh}$ and $\delta^{18}O_{carb\text{-}sh}$ increase with relative age (figs. 2 and 4I).

With the exception of some of the oldest samples, the $CaCO_3$ content of Group 3 shales is lower than shales from groups 1 and 2, ranging from 0.00–3.16 wt% (mean = 0.09 wt%, fig. 4J). Group 3 shales have TOC concentrations in the range 0.05–0.10 wt% (mean = 0.08 wt%, fig. 4K) and $CaCO_3$/TOC in the range 0.1–0.4 (mean = 0.11, fig. 4L). There is a significant positive correlation between $\delta^{13}C_{carb\text{-}sh}$ and $CaCO_3$ content (ρ = 0.57, p < 0.01, fig. 4J), but no significant correlation observed between $\delta^{13}C_{carb\text{-}sh}$ and TOC content (r = 0.56, p = 0.09, R^2 = 0.31 fig. 4K), or $\delta^{13}C_{carb\text{-}sh}$ and $CaCO_3$/TOC (ρ = -0.43, p = 0.29, fig. 4L).

4.4. Qualitative observations of $\delta^{13}C$ and $\delta^{18}O$ through the Nama Group

Carbonates that were deposited following initial transgressive onlap of the Nama basement record negative values of $\delta^{13}C_{carb}$ that correspond to the 'basal Nama excursion' (BANE; Bowyer et al., 2022; Maloney et al., 2020; Saylor et al., 1998; O. Smith, 1999; Wood et al., 2015). Following the BANE, $\delta^{13}C_{carb}$ values increase through the lower Omkyk Member (Zaris Sub-basin) and Kliphoek and Mooifontein members (Witputs Sub-basin), to reach peak values (~5‰) associated with the Omkyk excursion (OME, fig. 2; Bowyer et al., 2022; Saylor et al., 1998; O. Smith, 1999; Wood et al., 2015). Following the OME interval, $\delta^{13}C_{carb}$ values show a gradual decrease towards a minor negative excursion (Saylor et al., 1998). This interval has been tentatively correlated with a negative $\delta^{13}C_{carb}$ excursion recorded in the A0 Member of the Ara Group, Oman, based on a preliminary global chemostratigraphic correlation anchored by available radiometric data from tuff interbeds in the underlying Hoogland Member of the Nama Group and A0 Member of the Ara Group (Bowring et al., 2007). This negative excursion has therefore been termed the 'A0' excursion, for ease of reference (but see discussions of uncertainty in Bowyer et al., 2022 and O. Smith, 1999).

In the Schwarzrand Subgroup of the Witputs Sub-basin, carbonates of the lower Huns Member record recovery from a positive $\delta^{13}C_{carb}$ excursion (max $\delta^{13}C_{carb}$ = 4.24‰, section 1, fig. 2). This interval stratigraphically overlies the Nasep Member, wherein a tuff bed at a neighbouring section to the north of section 1 has been dated to 542.65 ± 0.15 Ma (Nelson et al., 2022). The $\delta^{13}C_{carb}$ peak recorded in the lower Huns Member at section 1 has been tentatively correlated with radiometrically-constrained positive $\delta^{13}C_{carb}$ values in the Tamengo Formation of Brazil (Boggiani et al., 2010; Parry et al., 2017) and the A3 Member of the Ara Group, Oman (Bowring et al., 2007). This interval of positive $\delta^{13}C_{carb}$ has therefore been termed the 'A3' excursion (Bowyer et al., 2022) but this is dependent upon the absolute age of the base of the Huns Member (see Discussion).

A compilation of all Nama Group carbonate data shows no correlation between $\delta^{13}C_{carb}$ and $\delta^{18}O_{carb}$ (ρ = -0.09, p <0.01, fig. 4M). However, individual sections and discrete intervals of the Nama Group record are characterized by significant correlation between $\delta^{13}C_{carb}$ and $\delta^{18}O_{carb}$ (fig. 2). As such, we consider associated temporal changes in $\delta^{13}C$ and $\delta^{18}O$, and differences in recorded values between carbonates and shales, through the Nama Group succession.

In the Kuibis Subgroup, Group 1 and Group 2 shales show generally reciprocal trends in $\delta^{13}C$ and $\delta^{18}O$ relative to carbonates within individual sections, and between contemporaneous sections, recording the BANE (fig. 2). Carbonates in the lowermost 10–20 m of this interval at sections 5, 8, 9 and 10, record increasing $\delta^{18}O_{carb}$ values that broadly covary with $\delta^{13}C_{carb}$ (fig. 2). Throughout this interval, $\delta^{13}C_{carb\text{-}sh}$ values of Group 1 shales at sections 9 and 10 and Group 2 shales at section 8, and $\delta^{18}O_{carb\text{-}sh}$ values of Group 1 shales at section 10 and Group 2 shales at section 8, covary in magnitude and trend with $\delta^{13}C_{carb}$ and $\delta^{18}O_{carb}$, respectively. Group 1 shales in the lowermost 10 m of section 9 record values of $\delta^{18}O_{carb\text{-}sh}$ that are more positive than interbedded $\delta^{18}O_{carb}$ (fig. 2). By contrast, in the Mara Member of the Witputs Sub-basin, carbonates at sections 6 and 7, and Group 1 shales at section 6, record scattered negative $\delta^{13}C$ values that correspond to the BANE, but show no positive correlation between $\delta^{13}C$ and $\delta^{18}O$ (fig. 2). Indeed, trends in $\delta^{13}C_{carb}$ and $\delta^{18}O_{carb}$ appear to be negatively correlated throughout this interval at section 7 (fig. 2).

Throughout the OME interval, there is no significant correlation between $\delta^{13}C_{carb}$ and $\delta^{18}O_{carb}$ in any section. Following the OME, $\delta^{13}C_{carb}$ values show a gradual decrease towards a minor negative excursion in the Urikos Member (or upper Hoogland Member) at one section to the northwest of section 9 (Zebra River, not shown on fig. 2), which is associated with positive correlation between $\delta^{13}C_{carb}$ and $\delta^{18}O_{carb}$ (Saylor et al., 1998).

Following the A3 excursion, carbonates of the Urusis Formation in the Witputs Sub-basin (sections 1–4, fig. 2) show limited variability in $\delta^{13}C_{carb}$ (-0.80‰ to 2.40‰, mean = 1.34‰, sd = 0.48) and no observable correlation between $\delta^{13}C_{carb}$ and $\delta^{18}O_{carb}$ (fig. 2). Values of $\delta^{18}O_{carb\text{-}sh}$ in Group 2 shales at sections 3 and 4 (-9.96‰ to -3.08‰, mean = -6.93‰, sd = 1.84) overlap with, or are more positive than, $\delta^{18}O_{carb}$ of approximately contemporaneous car-

bonates throughout this interval of the Neint Nababeep Plateau composite section (-9.39‰ to -4.87‰, mean = -6.99‰, sd = 1.15, figs. 2 and 4E).

In the Schwarzrand Subgroup of the Zaris Sub-basin, Group 3 shales at sections 11 and 12 are characterized by decreasing $\delta^{13}C_{carb\text{-}sh}$ and $\delta^{18}O_{carb\text{-}sh}$ up through the stratigraphic succession (fig. 2), and corresponding positive covariation between $\delta^{13}C_{carb\text{-}sh}$ and $\delta^{18}O_{carb\text{-}sh}$ (fig. 4I). These values are significantly depleted relative to $\delta^{13}C_{carb}$ and $\delta^{18}O_{carb}$ in samples of the contemporaneous mixed carbonate-clastic succession of the Witputs Sub-basin (sections 1–4, figs. 2, 4I).

5. DISCUSSION

5.1. $\delta^{13}C$ and $\delta^{18}O$ covariation and potential meteoric influence

Sedimentary rocks of the lower Kuibis Subgroup record diachronous deposition across basement rocks of the Kalahari craton in both the Zaris and Witputs sub-basins (Germs, 1974, 1983). As such, the thickest measured sections of the lower Nama Group that accumulated in the deeper parts of each sub-basin (e.g., sections 7 and 10) where accommodation space was greatest, also contain the oldest units. This is supported not only by lithostratigraphic and sequence stratigraphic correlation, but also by observations of $\delta^{13}C_{carb}$ chemostratigraphy and associated preliminary biostratigraphic considerations in both sub-basins (fig. 2; Bowyer, Uahengo, et al., 2023; Maloney et al., 2020; Saylor et al., 1995, 1998; O. Smith, 1999; Wood et al., 2015).

The oldest transgressive carbonates and shale-hosted carbonate cements at all studied sections record recovery from a negative $\delta^{13}C$ excursion (fig. 2). This interval is also characterized by a general shift in dominant lithology from dolostone to limestone, where the $\delta^{13}C$ trend is recorded in both dolostones and limestones within and between individual sections. In the lowermost 10–20 m of sections 5, 8, 9 and 10, this $\delta^{13}C_{carb}$ recovery is accompanied by significant $\delta^{13}C_{carb}$-$\delta^{18}O_{carb}$ covariation, with a corresponding increase in $\delta^{18}O_{carb}$ (fig. 2). By contrast, basal transgressive deposits of the Dabis Formation in the Witputs Sub-basin at sections 6 and 7 do not show any clear positive correlation between $\delta^{13}C_{carb}$ and $\delta^{18}O_{carb}$ (fig. 2). Carbonates of the Mara Member in section 6 are frequently characterized by evaporitic fabrics, and show scattered values of $\delta^{13}C_{carb}$ and $\delta^{18}O_{carb}$, whilst carbonates at section 7 show a general negative correlation between $\delta^{13}C_{carb}$ and $\delta^{18}O_{carb}$ through the lower ~50–75 m (fig. 2; Wood et al., 2015).

Carbonates of the lower Nama Group were most commonly deposited upon granitic basement rock, where the $\delta^{13}C$ of freshwater input was likely depleted due to the dominant influence of organic carbon respiration and lack of carbonate weathering that would otherwise contribute elevated $\delta^{13}C_{carb}$ (Khadka et al., 2014; Rodriguez Blanco et al., 2020). Positive $\delta^{13}C_{carb}$-$\delta^{18}O_{carb}$ covariation and low initial $\delta^{13}C_{carb}$ recorded in the lowermost 10–20 m of transgressive carbonate deposits in sections 5, 8, 9 and 10 may therefore reflect a greater degree of mixing between marine and freshwater associated with meteoric diagenesis. However, the overall trend from negative to positive $\delta^{13}C_{carb}$ recorded across the boundary between the Kanies and lower Omkyk members at section 10, and within the Kliphoek Member at sections 6 and 7, is accompanied by no synchronous positive shift in $\delta^{18}O_{carb}$ (fig. 2). Therefore, the degree to which meteoric diagenesis has altered $\delta^{13}C_{carb}$ from the composition of seawater DIC remains uncertain.

The recovery from a negative $\delta^{13}C_{carb}$ excursion recorded in dolostone of the Dengying Formation, South China, is radiometrically constrained to be <550.14 ± 0.63 Ma (Yang et al., 2021), and may correlate with the trend in $\delta^{13}C_{carb}$ recorded by carbonates of the lower Nama Group (Bowring et al., 2007; Saylor et al., 1998; Yang et al., 2021). However, $\delta^{13}C_{carb}$ values of the basal Nama Group are notably depleted relative to all other global $\delta^{13}C_{carb}$ data that postdate the Shuram $\delta^{13}C_{carb}$ excursion (*ca.* 575–565 Ma; Rooney et al., 2020; Yang et al., 2021) but pre-date the 1n/BACE. Therefore, if the BANE is distinct from the Shuram excursion, as suggested by current global chemostratigraphic age models (Bowyer et al., 2022; Bowyer, Uahengo, et al., 2023; Rooney et al., 2020; Yang et al., 2021), then the magnitude of the BANE may reflect regional amplification of negative $\delta^{13}C_{carb}$ values associated with local meteoric diagenesis.

Positive correlation between $\delta^{13}C_{carb}$ and $\delta^{18}O_{carb}$ is also recorded in carbonate interbeds of the Urikos Member (or upper Hoogland Member) of the Zebra River section (to the northwest of section 9), coincident with the inferred A0 negative $\delta^{13}C_{carb}$ excursion (Bowyer et al., 2022; Saylor et al., 1998). Lateral differences in $\delta^{13}C_{carb}$ recorded between sections in the vicinity of Zebra River, and meteoric dissolution of ooids observed within the upper Hoogland Member, have previously been suggested as possible evidence to support deviation of $\delta^{13}C_{carb}$ from the composition of seawater $\delta^{13}C_{DIC}$ in this interval associated with diagenetic alteration (O. Smith, 1999). Alternatively, the observed differences in trend and magnitude of $\delta^{13}C_{carb}$ between these sections may record lateral differences in section completeness associated with increasing paleodepth and accommodation space from southeast to northwest within the Zaris Sub-basin (for more information, see supplementary correlation chart of Bowyer, Uahengo, et al., 2023).

Group 3 shale samples in sections 11 and 12 also show positive covariation between $\delta^{13}C_{carb\text{-}sh}$ and $\delta^{18}O_{carb\text{-}sh}$, and decreasing values of both $\delta^{13}C_{carb\text{-}sh}$ and $\delta^{18}O_{carb\text{-}sh}$ during progressive infill and shallowing of the Zaris Sub-basin (figs. 2 and 4I). At this time, paleocurrent data indicate that clastic input to the Zaris Sub-basin was sourced from the present north and east (fig. 1C; Germs, 1983). Group 3 shales were deposited distant from the locus of carbonate sedimentation (Germs, 1983; Gresse & Germs, 1993; Saylor et al., 1995). Due to outcrop availability, samples were taken along road transects, and record increasing proximity to the source of clastic input with decreasing age (fig. 1C). As such, an increase in the contribution of isotopically light riverine freshwater to $\delta^{13}C_{carb\text{-}sh}$ with de-

creasing age appears to be the most parsimonious explanation for the significant deviation of $\delta^{13}C_{carb\text{-}sh}$ in Group 3 samples, relative to contemporaneous $\delta^{13}C_{carb}$ recorded throughout the carbonate-clastic succession of the Schwarzrand Subgroup in the Witputs Sub-basin (figs. 2, 4I).

5.2. Potential significance of $\delta^{13}C_{carb\text{-}sh}$ data from carbonate-clastic successions

The isotopic composition of marine carbonates is commonly considered to approximate the isotopic composition of DIC in seawater, provided that precipitated carbonate minerals have not undergone significant subsequent diagenetic alteration. In the Kuibis Subgroup, whole rock carbonates and carbonate cements within Group 1 and Group 2 shales show $\delta^{13}C$ values that are consistent in magnitude and trend (fig. 2). We may infer this to reflect a consistent source for the measured carbonate, potentially seawater DIC.

Nama Group reef carbonates from the Omkyk Member show multiple phases of syndepositional through to late burial cements (Wood et al., 2018), but the timing and type of carbonate cements found in Nama Group clastics is not known, and indeed these may potentially have formed at any time during diagenesis, and from any diagenetic fluid. $\delta^{13}C$ and $\delta^{18}O$ values will only show a correlation in scenarios where there is mixing between different end-members of alteration or by mixing of two different diagenetic fluids. For example, in meteorically-altered carbonates the most altered end-member will have low $\delta^{13}C$ and $\delta^{18}O$, while the least altered end-member will show high $\delta^{13}C$ and $\delta^{18}O$ values relative to contemporaneous seawater DIC, and a similar trend can also be created by mixing of two different diagenetic fluids such as seawater and meteoric water. Values of $\delta^{13}C_{carb\text{-}sh}$ from Group 1 and 2 shales in carbonate-clastic successions show no significant correlation with $\delta^{18}O_{carb\text{-}sh}$, which may suggest that they formed from a single diagenetic fluid and during a single diagenetic stage (fig. 4A, E). By contrast, Group 3 shales in clastic-only successions show a statistically significant positive correlation between $\delta^{13}C_{carb\text{-}sh}$ and $\delta^{18}O_{carb\text{-}sh}$, and more negative and variable $\delta^{13}C_{carb\text{-}sh}$ values than contemporaneous $\delta^{13}C_{carb}$ (fig. 4I), and so may therefore have formed by either a mixture of variably diagenetically-altered end-members, or via the mixing of two different diagenetic fluids.

5.3. $\delta^{13}C_{carb\text{-}sh}$, organic carbon and $CaCO_3$ content

Bulk $\delta^{13}C$ values derived from impure carbonates can deviate from the composition of seawater DIC due to the incorporation of organic matter and subsequent formation of authigenic carbonate during diagenesis. This deviation is most likely to occur in sediments with low carbonate content relative to organic carbon (Saltzman & Thomas, 2012). Scattered negative $\delta^{13}C_{carb}$ values recorded from samples of the Neint Nababeep Plateau composite section have also been associated with stratigraphic proximity to siliciclastic-rich intervals, and they have thus not been considered useful for basin-wide $\delta^{13}C$ correlation (Nelson et al., 2022).

Group 1 and 2 shales were deposited in settings where CO_3^{2-} concentrations are inferred to have been high, consistent with contemporaneous, laterally extensive carbonate platform development. In such settings, authigenic carbonate may readily precipitate from seawater. Clastic-hosted carbonate cements from samples of the mixed carbonate-clastic Isaac Formation of the Ediacaran Windermere Supergroup of Laurentia have similarly been shown to record $\delta^{13}C$ values that approximate contemporaneous $\delta^{13}C_{carb}$ (Canfield et al., 2020; Cochrane et al., 2019). We infer that seawater was the primary DIC source for precipitation of carbonate cements in Group 1 shales given elevated concentrations of $CaCO_3$ (0.02–11.96 wt%, mean = 1.77 wt%) compared to Group 3 shales from clastic-only successions (0.00–3.16 wt%, mean = 0.22 wt%), and the consistency between $\delta^{13}C_{carb\text{-}sh}$ in Group 1 shales and $\delta^{13}C_{carb}$ from associated, interbedded carbonates (figs. 2 and 4A). Group 2 shales have an intermediate range of $CaCO_3$ concentrations (0.00–4.43 wt%) relative to shales from groups 1 and 3, and a mean $CaCO_3$ concentration (1.05 wt%) that is elevated relative to Group 3 shales. The median $CaCO_3$ concentration of Group 2 shales (0.89 wt%) is also significantly elevated relative to Group 1 (0.18 wt%) and Group 3 (0.01 wt%) shales. Despite these observations, Group 2 shales of the Schwarzrand Subgroup record $\delta^{13}C_{carb\text{-}sh}$ values that are depleted relative to carbonates above and below the sampled shale package in section 3 and below the sampled shale package at section 4 (fig. 2). If seawater was the primary DIC source for carbonate cement precipitation in Group 2 shales, then the apparent deviation of $\delta^{13}C_{carb\text{-}sh}$ from approximately contemporaneous $\delta^{13}C_{carb}$ in sections 3 and 4 might be a consequence of contamination by additional ^{12}C associated with elevated TOC, and this is explored below.

The combined shale data from groups 1–3 show a significant positive correlation between $\delta^{13}C_{carb\text{-}sh}$ and $CaCO_3$ (ρ = 0.69, $p < 0.01$, fig. 4N), and a moderate but statistically significant negative correlation between $\delta^{13}C_{carb\text{-}sh}$ and TOC (ρ = -0.43, p = 0.01, fig. 4O). These correlations appear to support the inference that samples of lower purity (characterized by low $CaCO_3$/TOC, fig. 4P) will tend to record more negative $\delta^{13}C_{carb\text{-}sh}$. However, given the low TOC concentrations of shales from the Nama Group (<0.20 wt%), the power of these statistical correlations are impacted to a degree by analytical uncertainties associated with TOC measurements (precision of better than ±0.04 wt%; Bowyer et al., 2020). Future studies that aim to further test this hypothesis would therefore benefit from sample sets with a larger range in TOC concentrations.

A carbonate to organic carbon concentration ratio of 7:1 has been suggested as a potential threshold below which the incorporation of ^{12}C from organic matter may result in deviation of bulk $\delta^{13}C$ from the composition of seawater DIC (Saltzman & Thomas, 2012). Indeed, very low $CaCO_3$/TOC ratios (0.06–0.36) in Group 3 shales may be partly responsible for the clearly depleted $\delta^{13}C_{carb\text{-}sh}$ relative to contemporaneous $\delta^{13}C_{carb}$ (fig. 4I). However, val-

ues of $\delta^{13}C_{carb\text{-}sh}$ in Group 1 shales clearly track the magnitude and trend of $\delta^{13}C_{carb}$ recorded by carbonate interbeds (fig. 2). These, after removing one outlier ($CaCO_3$/TOC = 84.99), have a mean $CaCO_3$/TOC of 3.70 (fig. 4D). The average purity of Group 2 shales (mean $CaCO_3$/TOC = 18.49, n = 12) is greater than Group 1 shales, even when this outlier value is included (mean = 11.83, n = 10, figs. 4D, H, P). It is therefore difficult to disregard values $\delta^{13}C_{carb\text{-}sh}$ derived from Group 2 shales, which are more negative than average $\delta^{13}C_{carb}$ of coeval carbonates in the Urusis Formation, on the basis of sample purity alone. We therefore explore the lithostratigraphic correlation of the Schwarzrand Subgroup in the vicinity of sections 3 and 4, in order to investigate the stratigraphic position of negative $\delta^{13}C_{carb\text{-}sh}$ data from Group 2 shales relative to regional $\delta^{13}C_{carb}$ chemostratigraphy.

5.4. Implications of alternative lithostratigraphic correlations for regional chemostratigraphy

The Urusis Formation in the Witputs Sub-basin is a mixed carbonate-siliciclastic succession deposited over a *ca.* 4-million-year period from ⩽543 Ma to ⩾538.5 Ma (Linnemann et al., 2019; Nelson et al., 2022; Saylor et al., 1998). Extensive studies of litho-, chemo-, bio- and sequence stratigraphy, alongside radiometric dating of the Urusis Formation succession, have focused on sections that outcrop on farms Nord Witputz 22, Swartpunt 74 and Swartkloofberg 95 (fig. 5; Darroch et al., 2015; Grotzinger et al., 1995; Jensen et al., 2000; Linnemann et al., 2019; Saylor et al., 1998; Saylor & Grotzinger, 1996; Wood et al., 2015). Confident lithostratigraphic correlation of strata in this region is complicated by laterally discontinuous outcrop associated with eroded topography, and the recognition of regional thrust faulting and folding associated with the Gariep Orogeny (fig. 5A; Saylor & Grotzinger, 1996). Here, we present four possible lithostratigraphic correlations for sections 1–4 (fig. 5B), which result in a range of possible chemostratigraphic correlations for the $\delta^{13}C_{carb\text{-}sh}$ data in section 4 relative to the radiometrically constrained Nama Group composite $\delta^{13}C_{carb}$ age framework. Each of these four lithostratigraphic correlations are discussed below.

Correlation 1 corresponds to the original lithostratigraphic correlation of Saylor and Grotzinger (1996) wherein the extended shale package at section 4 is correlated with the Feldschuhhorn Member (fig. 5B). This was justified by Saylor and Grotzinger (1996) on the basis of correlating an underlying unit of pink thrombolitic and stromatolitic lime mudstone at section 4 to a lithologically similar unit in the upper Huns Member at sections further to the east. According to this correlation, available radiometric data would constrain the negative $\delta^{13}C_{carb\text{-}sh}$ data recorded at section 4 to between 542.65 ± 0.15 Ma and 540.095 ± 0.099 Ma (Linnemann et al., 2019; Nelson et al., 2022), however the precise age and duration of the Feldschuhhorn Member within this interval remains uncertain. This is further complicated by uncertainties in the reliability of available radiometric ages and lithostratigraphic correlation between sections 2 and 3

Recent re-dating of an ash bed within section 2 has been preliminarily interpreted to suggests that this section may have been laterally equivalent to, rather than stratigraphically beneath, section 3 (Messori et al., 2021). Sections 2 and 3 show consistency in lithostratigraphic architecture and number of ash beds (fig. 5B). However, Nelson et al. (2022) suggest that the age of the lowermost ash bed in section 3 (dated at 540.095 Ma, Linnemann et al., 2019) may instead represent a maximum depositional age. If future structural reassessments allow for sections 2 and 3 to represent laterally equivalent depositional successions, then section 2 may have been deposited in a shallower depositional environment than section 3 based on the available sedimentological details. However, out-of-sequence ages of ash beds in the vicinity of Farm Swartpunt associated with possible zircon reworking in the source magma chamber(s) cannot presently be ruled out. The lithostratigraphic and radiometric correlation between sections 2 and 3 demands future clarification, as it has significant implications for the duration of Huns Member deposition in the Witputs Sub-basin, lithostratigraphic subdivision, and lateral differences in sedimentation rate. Differences in sedimentation rate between correlative sections also have significant implications for interpretations of associated geochemical proxy data (Nelson et al., 2022). Integrated stratigraphic, geochemical, and radiometric dating may resolve these ongoing uncertainties.

Correlation 2 implies that the extended shale package at section 4 is equivalent to the transgressive systems tract of medium scale sequence E17 of Saylor (2003), which immediately underlies section 3. Given the uncertainty in lithostratigraphic correlation between sections 2 and 3, this would result in an age range for the section 4 $\delta^{13}C_{carb\text{-}sh}$ data equivalent to, or slightly younger than, correlation 1, but still ⩾540.095 ± 0.099 Ma, if this is the accepted depositional age of the lowermost ash bed in section 3 (fig. 5B, but see Nelson et al., 2022). Alternatively, correlation 3 implies that the two extended shale packages in sections 3 and 4 are coeval, but were deposited at significantly different depositional rates, and that both are <538.99 ± 0.21 Ma (Linnemann et al., 2019).

Lastly, correlation 4 re-positions section 4 stratigraphically above section 3, and implies that the negative $\delta^{13}C_{carb\text{-}sh}$ data in section 4 are younger than the negative $\delta^{13}C_{carb\text{-}sh}$ data in section 3, <538.99 ± 0.21 Ma (fig. 5B; Linnemann et al., 2019). Despite the recognition of thrust faulting in this area, this correlation also appears to be the most parsimonious when considering the consistent regional dip to the north/northwest for sections to the east of the large NW–SE trending fold and fault system to the west of section 4 (figs. 5A and 6). Correlation 4 would simply assume a less significant offset associated with the thrust fault that separates sections 3 and 4 (fig. 6D). Linnemann et al. (2019) note that tuff bed 6 may be reworked, and indeed if this reworking is from the underlying Spitskop Member (now removed by erosion), then the onset of the $\delta^{13}C_{carb\text{-}sh}$ excursion at section 4 may be younger than 538.6 Ma. A possible further alternative stratigraphic correlation (not shown in fig. 5) would imply that the entire

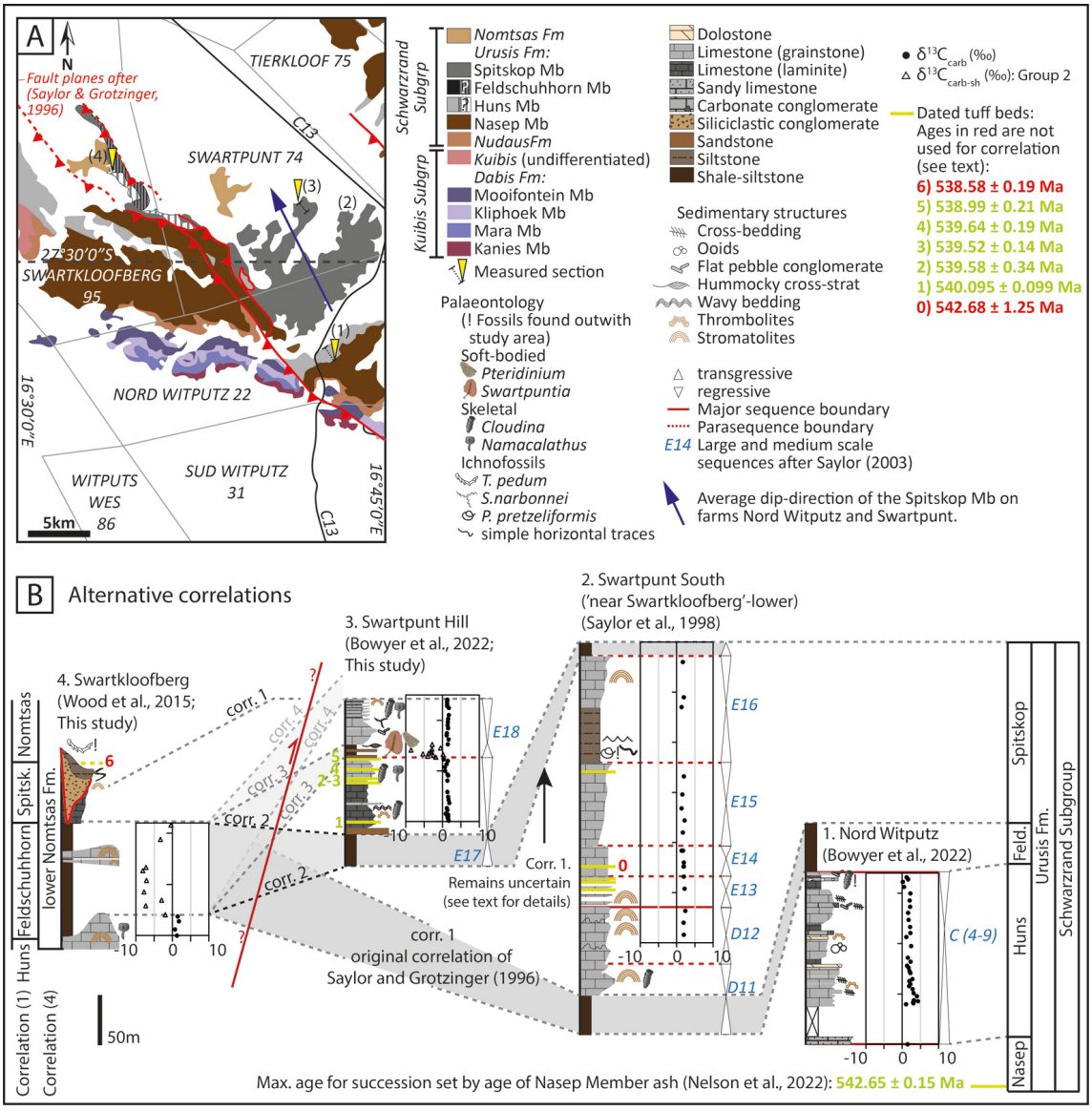

Figure 5. Possible lithostratigraphic correlations for sections of the Urusis Fm in the Witputs Sub-basin on farms Swartkloofberg, Swartpunt and Nord Witputz.

(A) Geological map showing locations of sections 1 to 4. Map redrawn from Saylor and Grotzinger (1996), with additional geological information from the 1:250000 map of AI-AIS (2716), Geological Survey of Namibia, Ministry of Mines and Energy. (B) Correlations 1–4, discussed in the main text. Corr. 1 follows original lithostratigraphic correlation of Saylor and Grotzinger (1996). Medium scale sequences C4 to E18 after Saylor (2003). Ash bed ages after Grotzinger et al. (1995, recalculated in Schmitz, 2012), Linnemann et al. (2019), and Nelson et al. (2022). Ash beds 0 and 6 are not considered useful for correlation (see text for details). Lithostratigraphic and/or radiometric correlation between sections 2 and 3 remains uncertain after observations of Messori et al. (2021) and Nelson et al. (2022) (see text for details). Correlation 4 implies that ash bed (6) is likely redeposited (Linnemann et al., 2019). Feld. = Feldschuhhorn Mb, Spitsk. = Spitskop Mb.

Feldschuhhorn Member at section 4 corresponds to ongoing deep water shale deposition equivalent to the entirety of the Feldschuhhorn and Spitskop members in shallower sections 1–3.

Correlation 4 may find further support in recent high resolution litho-, bio- and $\delta^{13}C_{carb}$ chemostratigraphic assessment, and radiometric dating of correlative strata on the Neint Nababeep Plateau that were deposited in the Vioolsdrif Sub-basin (Nelson et al., 2022). Figure 7 shows two possible litho- and chemostratigraphic correlations between all relevant sections of the Urusis and Nomtsas formations in the Witputs and Vioolsdrif sub-basins. In this figure, the lithostratigraphic correlation of Witputs Sub-basin sections follows correlation 4. The two lithostratigraphic correlations between the Witputs and Vioolsdrif sub-basins have different implications for rates of sediment accumulation in the Witputs sub-basin (fig. 8).

Nelson et al. (2022) interpret the age of ash bed 1 at section 3 as a maximum depositional age and correlate the lower carbonate-dominated unit of the Neint Nababeep Plateau to the Huns Member (fig. 7). However, if ash beds 1–5 at section 3 approximate the ages of deposition, as originally proposed (Linnemann et al., 2019), then the implication is that the entire carbonate-dominated Huns-Spitskop members of the composite Neint Nababeep Plateau succession instead correspond to an expanded lateral equivalent of the Spitskop Member in the Witputs Sub-basin (correlation 5 in figs. 7C, 8). Whilst possible, this

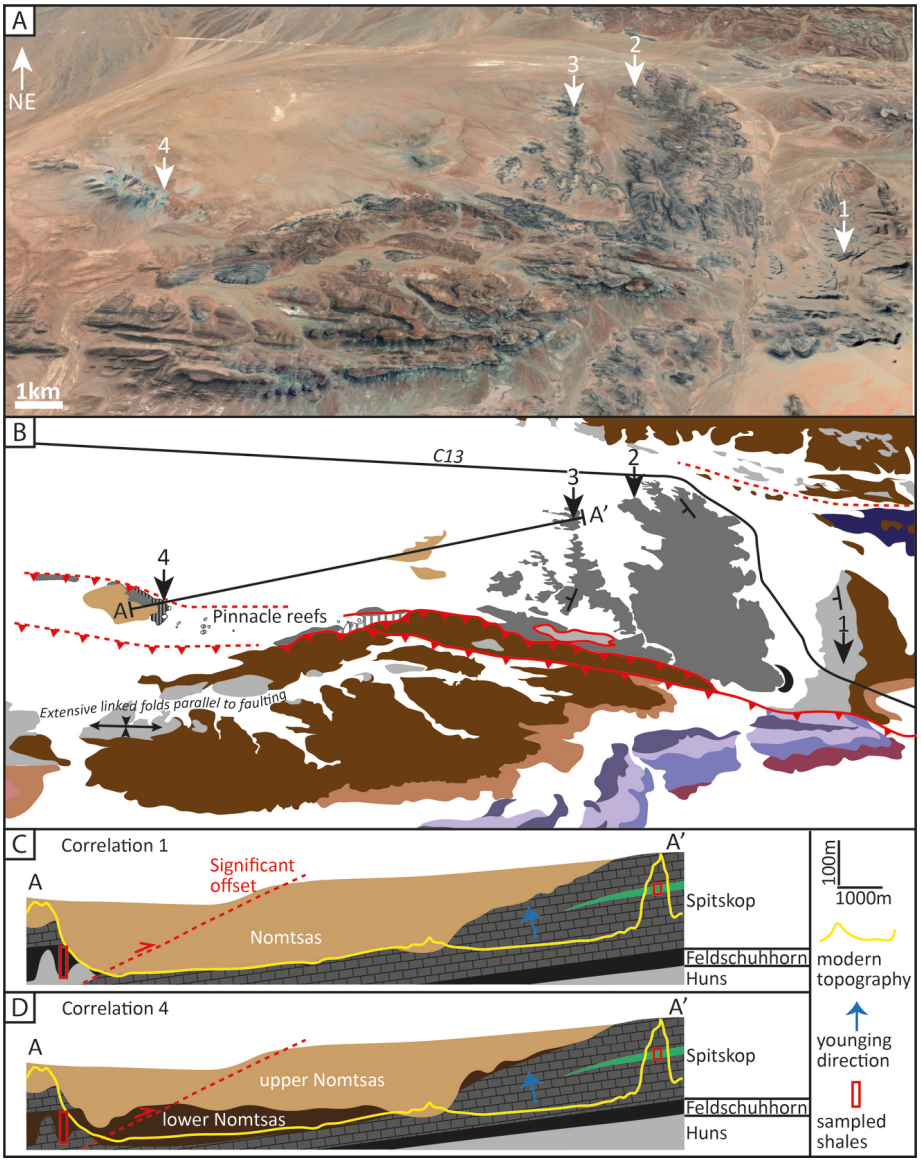

Figure 6.

(A) Inclined satellite image of strata that outcrop in the vicinity of sections 1 to 4 (GoogleEarth). See fig. 5A for coordinates and reoriented map. (B) Geological map of (A) modified and simplified after Saylor and Grotzinger (1996) and 1:250000 map of AI-AIS area (2716) Geological Survey of Namibia, Ministry of Mines and Energy. Colors of geological units correspond to key in figure 5A. (C), (D): Schematic cross-sections A–A' after possible lithostratigraphic correlations, following (C) correlation 1 of Saylor and Grotzinger (1996), and (D) correlation 4 (herein).

would imply that, in the Neint Nababeep Plateau succession, time-equivalent deposits to the Huns Member are dominantly siliciclastic (correlation 5 in figs. 7C, 8). In this correlation, the lithostratigraphic architecture, $\delta^{13}C_{carb}$ -chemostratigraphy, and radiometric ages of the Neint Nababeep Plateau succession also appear consistent with lateral correlation to the Spitskop Member and lower Nomtsas Formation in sections 1–4, to the north, which were themselves deposited more slowly (correlation 5, figs. 7B, C, 8). Unfortunately, the largely invariant $\delta^{13}C_{carb}$ data throughout this interval make this correlation difficult to verify chemostratigraphically. Adopting correlation 4 for sections of the Witputs Sub-basin and either the original correlation of Nelson et al. (2022) or correlation 5 between the Witputs and Vioolsdrif sub-basins, also allows for basin-wide transgression and the contemporaneous development of pinnacle reefs of the lower Nomtsas Formation at section 4 and the Neint Nababeep Plateau (fig. 7C). This would, by extension, imply that the fragmented ash bed at section 4 (538.58 ± 0.19 Ma, Linnemann et al., 2019) is redeposited from the uppermost Spitskop Member. The veracity of correlation 5 requires future verification of the lithostratigraphic and radiometric correlation between sections 2 and 3 (e.g., Messori et al., 2021; Nelson et al., 2022), particularly by integration of data from core with outcrop.

5.5. Calibrating $\delta^{13}C_{carb\text{-}sh}$ data within the current terminal Ediacaran age framework

Nelson et al. (2022) record relatively stable, positive $\delta^{13}C_{carb}$ values throughout the Neint Nababeep Plateau section, with scattered negative values that may be laterally correlative with negative $\delta^{13}C_{carb\text{-}sh}$ values at section 3, documented herein (figs. 8, 9). This may also imply that the

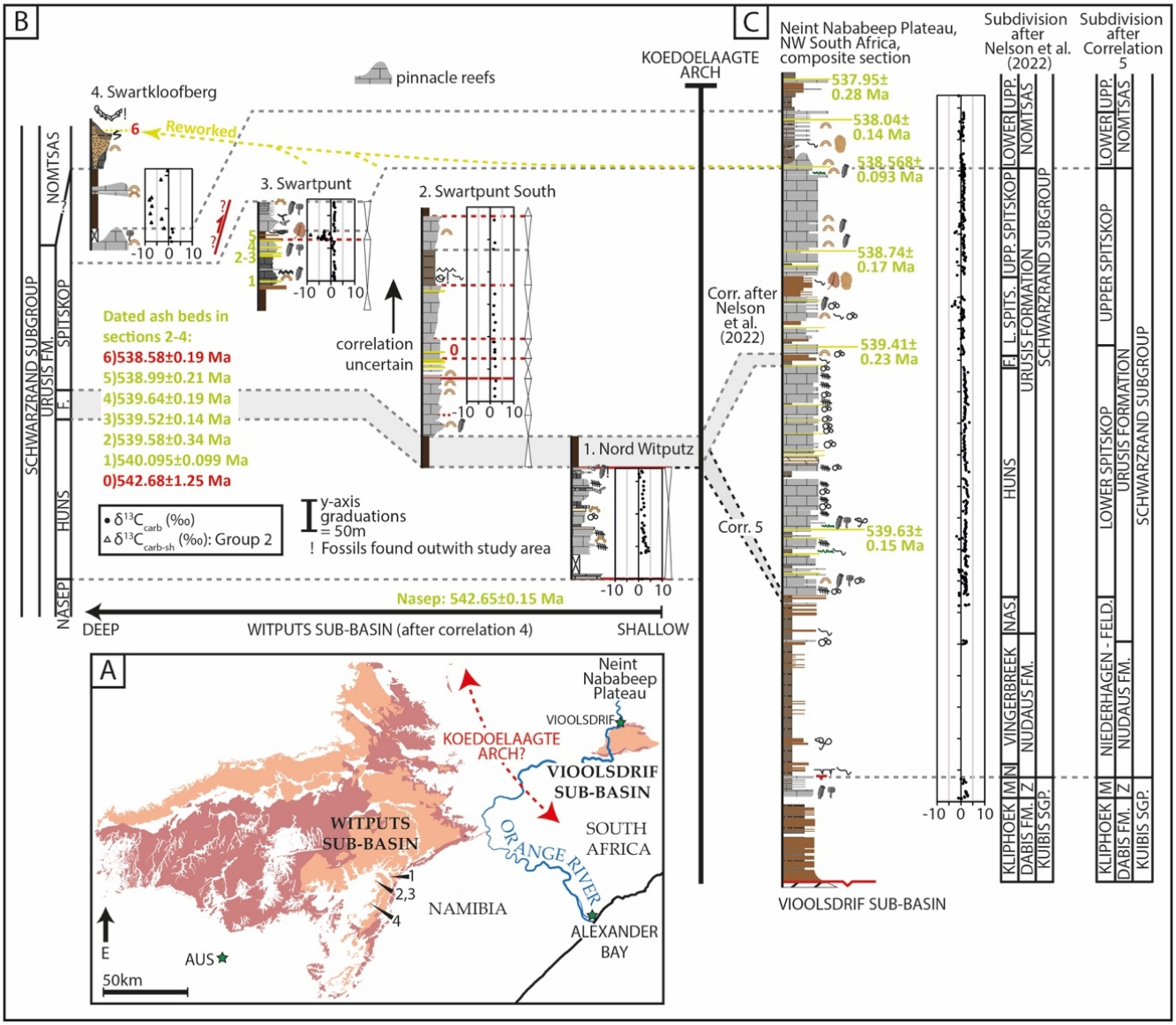

Figure 7.

(A) Simplified geological map of the Witputs and Vioolsdrif sub-basins to show positions of studied sections of the Urusis Formation (dashed red arrows are parallel to the hinge line of the possible flexural forebulge of the Koedoelaagte Arch after Germs & Gresse, 1991). (B) Litho- and chemostratigraphic correlation of study sections 1 to 4 in the Witputs Sub-basin, after correlation 4 (fig. 5B). Section information and data from Saylor et al. (1998), Wood et al. (2015), Bowyer et al. (2022) and this study. (C) Litho- and chemostratigraphic correlation of the composite Neint Nababeep Plateau section, showing Formation and Member subdivision after Nelson et al. (2022), and possible alternative subdivision of correlation 5, herein (see text for discussion). Ash bed ages after Grotzinger et al. (1995, recalculated in Schmitz, 2012), Linnemann et al. (2019), and Nelson et al. (2022). Ash beds 0 and 6 are not considered useful for correlation (see text for details). All sections to scale.

magnitude of negative $\delta^{13}C_{carb\text{-}sh}$ in Group 2 shales at section 3 is exaggerated relative to contemporaneous $\delta^{13}C_{carb}$, possibly associated with sample impurity (Nelson et al., 2022). However, given the uncertainty in the lithostratigraphic correlation of section 4, it remains possible that $\delta^{13}C_{carb\text{-}sh}$ data recorded by Group 2 shales at section 4 reflect trends in seawater $\delta^{13}C_{DIC}$.

A composite chemostratigraphic curve for the Nama Group has been constructed via visual alignment of $\delta^{13}C_{carb}$ data within the well-established litho- and chemostratigraphic framework of the Kuibis and Schwarzrand subgroups, and temporally constrained by all available radiometric ages within and between sections (fig. 9, full details of the methodological approach and associated uncertainties are provided in Bowyer et al., 2022; Bowyer, Uahengo, et al., 2023; Bowyer, Zhuravlev, et al., 2023). Within this framework, three chemostratigraphic alignments for section 4 result from lithostratigraphic correlations 1 to 4 of the Urusis Formation in the Witputs Sub-basin, and correlation 5 between the Witputs and Vioolsdrif sub-basins (fig. 9). In lithostratigraphic correlations 1 and 2, radiometric ages of 542.65 Ma and 540.099 Ma that bracket deposition of (at maximum) the upper Nasep, Huns and Feldschuhhorn members (Linnemann et al., 2019; Nelson et al., 2022) would correlate the $\delta^{13}C_{carb\text{-}sh}$ data at section 4 with radiometrically-constrained negative $\delta^{13}C_{carb}$ data in the A4 Member of the Ara Group, Oman (figs. 9A–C; Bowring et al., 2007). However, it now appears most likely that the radiometric age from the ash bed in the basal A4 Member does not constrain the onset age of this excursion

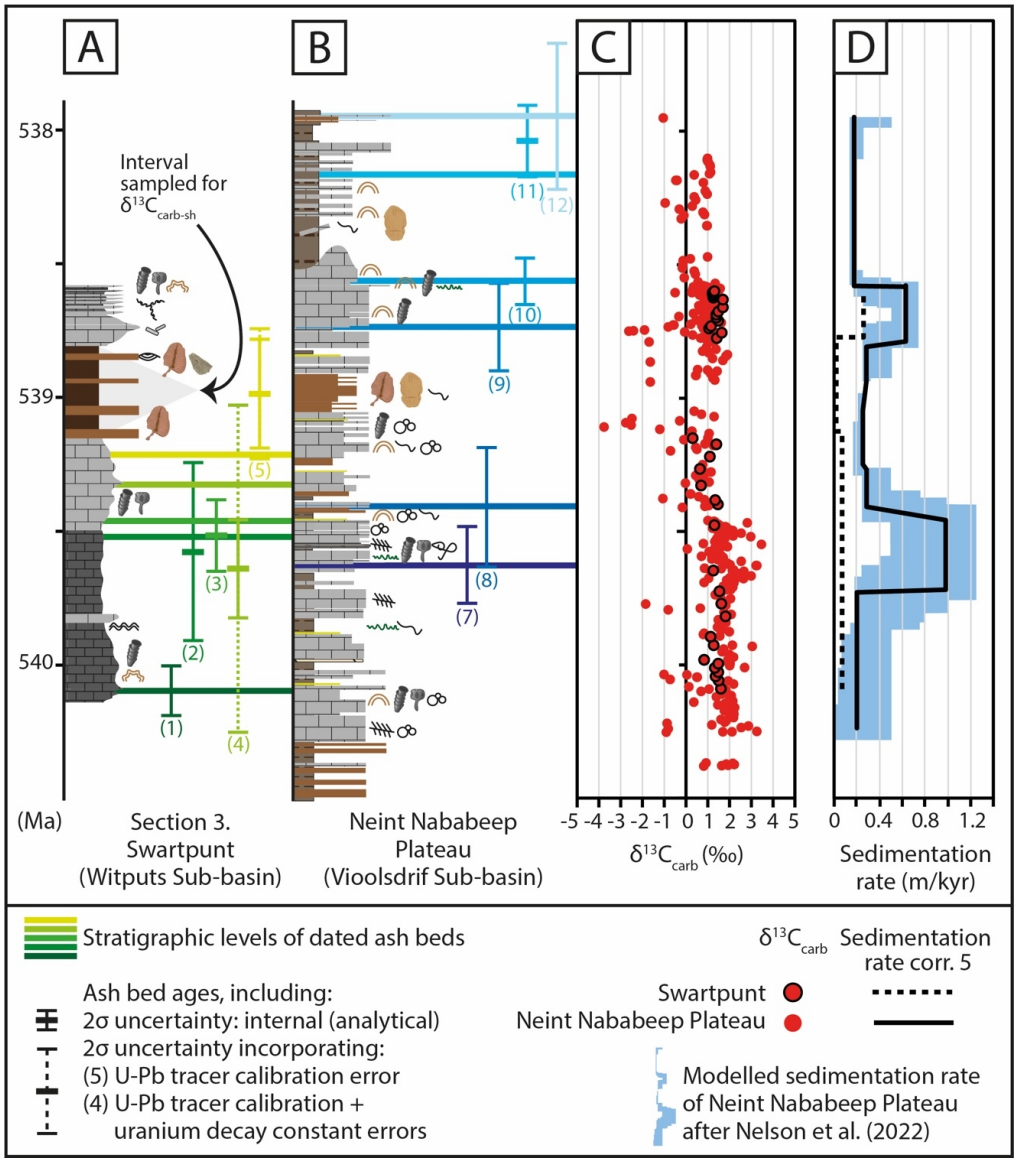

Figure 8. Temporal calibration of litho-, bio- and chemostratigraphy between (A) Swartpunt (section 3) and (B) the Neint Nababeep Plateau composite section according to correlation 5.

Colored horizontal bars show the lithostratigraphic positions of dated ash beds used for calibration (ash beds 1–5: Swartpunt section; ash beds 7–11: Neint Nababeep Plateau). The age of each ash bed level is shown relative to the corresponding position within the uncertainty of each associated radiometric age (colored vertical bars). Ash beds 4 and 5 fall outside of analytical uncertainty, but within total uncertainty, of their associated radiometric ages. (C) $\delta^{13}C_{carb}$ chemostratigraphy between Swartpunt (section 3) and the Neint Nababeep composite section according to correlation 5. (D) The difference in sedimentation rate between Swartpunt (section 3) and the Neint Nababeep Plateau composite section that results from correlation 5, superimposed upon the modeled sedimentation rate for the Neint Nababeep Plateau composite section after Nelson et al. (2022). Key to litho- and biostratigraphy provided in figure 2. Radiometric ages are from Linnemann et al. (2019) and Nelson et al. (2022). $\delta^{13}C_{carb}$ data from Bowyer et al. (2022) and Nelson et al. (2022).

(see Nelson et al., 2023), and that the putative 'A4 excursion' does not exist in this temporal window. By contrast, lithostratigraphic correlation 3 results in direct correlation between $\delta^{13}C_{carb-sh}$ data at sections 3 and 4 (fig. 9D). In both correlations, $\delta^{13}C_{carb-sh}$ values are significantly depleted relative to $\delta^{13}C_{carb}$ and cannot be considered informative of any trend in seawater $\delta^{13}C_{DIC}$.

The 1n/BACE has not been recorded in the Witputs or Vioolsdrif sub-basins (fig. 7) and associated data therefore likely support a 1n/BACE onset after 538.04 ± 0.14 Ma (Nelson et al., 2022, 2023), consistent with age models C to F of Bowyer et al. (2022) and Bowyer, Zhuravlev et al. (2023) and age model K of Bowyer, Uahengo, et al. (2023). If $\delta^{13}C_{carb-sh}$ values of Group 2 shales at section 4 approximate the trend of seawater $\delta^{13}C_{DIC}$, then lithostratigraphic correlation 4 suggests that the apparent negative $\delta^{13}C_{carb-sh}$ excursion recorded at section 4 may correlate with an unnamed excursion that predates the 1n/BACE, and is <538.04 Ma (fig. 9E; see Bowyer, Uahengo, et al., 2023; Nelson et al., 2022, 2023). These data may correspond in time with the negative $\delta^{13}C_{carb}$ excursion recorded in the lower Zuun-Arts Formation of Mongolia (e.g., E. F. Smith, Macdonald, et al., 2016; Topper et al., 2022) but the global significance of this excursion currently remains uncertain due to a dearth of radiometrically calibrated $\delta^{13}C_{carb}$ data ca. 538–535 Ma. However, similar to correlations 1-3, correlation 4 also implies that the $\delta^{13}C_{carb-sh}$ data in section 4 are depleted relative to contemporaneous $\delta^{13}C_{carb}$. We note

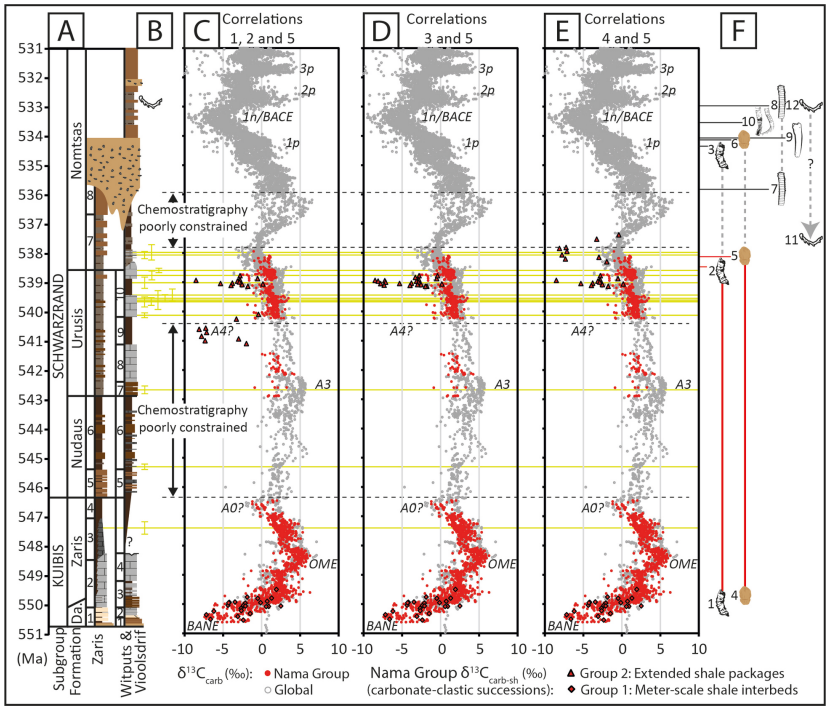

Figure 9. Updated radiometrically-calibrated lithostratigraphic and $\delta^{13}C_{carb}$ chemostratigraphic age models (A-E) for the Nama Group succession of Namibia and northwest South Africa (red data points) superimposed upon possible global $\delta^{13}C_{carb}$ age framework (grey circles after Model K of Bowyer, Uahengo, et al., 2023, updated after Nelson et al., 2023).

(F) 1. Minimum age for lowest occurrence of *Cloudina* in the Nama Group (Bowyer, Uahengo, et al., 2023); 2. Minimum age for last occurrence of *Cloudina* in the Nama Group (538.47 Ma), calibrated within the Bayesian age-depth model of Nelson et al. (2022); 3. Last occurrence of cloudinids at Mount Dunfee, Nevada (Nelson et al., 2023; E. F. Smith, Nelson, et al., 2016); 4. Lowest occurrence of soft-bodied fossils of the classic Nama assemblage in the Nama Group; 5. Minimum age for last occurrence of erniettomorphs in the Nama Group (538.16 Ma), calibrated within the Bayesian age depth model of Nelson et al. (2022); 6. Last occurrence of erniettomorphs at Mount Dunfee, Nevada (Nelson et al., 2023; E. F. Smith, Nelson, et al., 2016); 7. Lowest occurrence of cloudinid *Zuunia chimidtsereni* at Bayan Gol, Zavkhan Terrane, Mongolia (Topper et al., 2022); 8. Last occurrence of *Z. chimidtsereni* at Bayan Gol (Topper et al., 2022); 9. Conservative estimate for lowest occurrence of simple anabaritids (*Cambrotubulus*) in Siberia (Bowyer, Uahengo, et al., 2023; Bowyer, Zhuravlev, et al., 2023); 10. Chemostratigraphic position of cloudinids *Saarina* and *Costatubus* at Mount Dunfee, Nevada (Selly et al., 2020; E. F. Smith, Nelson, et al., 2016); 11. Lowest possible occurrence of *T. pedum* in the Nama Group (538.23 Ma), based on its apparent absence from strata of the Neint Nababeep Plateau composite section; 12. Approximate age for lowest occurrence of *T. pedum* coincident with peak 1.5p/2p at Mount Dunfee, Nevada (Nelson et al., 2023; E. F. Smith, Nelson, et al., 2016).

that lithostratigraphic correlation 4, whereby pinnacle reefs developed contemporaneously at section 4 and the Neint Nabebeep Plateau, remains possible even if $\delta^{13}C_{carb\text{-}sh}$ at section 4 are not considered useful for chemostratigraphy.

5.6. Potential biostratigraphic considerations and future target intervals

A preliminary global biostratigraphy has been constructed for the Ediacaran-Cambrian transition, which calibrates first and last appearances of key fossils directly within the global $\delta^{13}C_{carb}$ chemostratigraphic age framework (fig. 9C–F; Bowyer, Uahengo, et al., 2023). This age framework is undergoing continuous calibration with the publication of new data and lithostratigraphic considerations (e.g., Bowyer, Zhuravlev, et al., 2023; Nelson et al., 2023; Topper et al., 2022), and may be a useful predictive tool for targeting uncertain intervals of the stratigraphic record for geochemical and paleontological sampling. For example, the output of each age framework allows visualization of the series of biotic first and last appearances across the 1n/BACE interval and may help to inform targeted sampling of stratigraphic intervals in order to clarify temporal and spatial distributions of critical transitional biota.

The Bayesian age-depth model of Nelson et al. (2022) constrains ages for the last appearances of erniettomorphs and *Cloudina* in the Neint Nababeep Plateau composite section (fig. 9F) and also permits the calculation of uncertainties for each age. In contrast to Bayesian age-depth models, uncertainties in the precise ages of biotic first and last appearances are difficult to constrain by visual $\delta^{13}C_{carb}$ alignment alone, especially when considering local effects, including diagenesis, on regional $\delta^{13}C_{carb}$ variability. However, it is possible to make broad observations concerning the chemostratigraphic position of biotic first and last appearances relative to large magnitude $\delta^{13}C_{carb}$ excursions such as the 1n/BACE, if long-term trends in $\delta^{13}C_{carb}$ within each succession reflect changes in global seawater $\delta^{13}C_{DIC}$.

The lowest occurrence of the cloudinid *Zuunia chimidtsereni* in the Zuun-Arts Formation of the Zavkhan Terrane, Mongolia pre-dates negative $\delta^{13}C_{carb}$ values associated with the regional expression of the 1n/BACE (Topper et al., 2022). Visual $\delta^{13}C_{carb}$ alignment of the Zavkhan and Laurentian successions of Nevada and California, with associated uncertainties, may permit a degree of temporal overlap between the maximum first appearance of *Z. chimidtsereni*

and a terminal Ediacaran cloudinid assemblage, including (but not limited to) *Saarina* and *Costatubus* (fig. 9F; Bowyer, Uahengo, et al., 2023; Nelson et al., 2023; Selly et al., 2020; E. F. Smith, Nelson, et al., 2016; Topper et al., 2022). A conservative maximum age for the first appearance of morphologically simple anabaritids in Siberia is set by fossils assigned to *Cambrotubulus* within the Turkut Formation of the Olenek Uplift, which stratigraphically underlie the onset of a negative $\delta^{13}C_{carb}$ excursion interpreted to correlate with the 1n/BACE (fig. 9F; Bowyer, Zhuravlev, et al., 2023; Pelechaty et al., 1996; Rogov et al., 2015). Therefore, the present global age framework appears to suggest that the terminal Ediacaran cloudinid assemblage, and morphologically simplest anabaritids, post-date deposition of the lowermost Nomtsas Formation of the Nama Group (fig. 9).

Given that the maximum age for the onset of the 1n/BACE remains uncertain, and notwithstanding possible issues associated with endemism of terminal Ediacaran to lower Cambrian skeletal fossils, this age framework suggests that tubular fossils that predate the 1n/BACE in Laurentia (e.g., Selly et al., 2020) and Mongolia (e.g., Topper et al., 2022), may yet be identified within the youngest interbedded carbonate-siliciclastic units of the Nomtsas Formation that predate the regional erosional unconformity. According to lithostratigraphic correlation 4, herein, strata of the Nomtsas Formation in section 4 and the Neint Nababeep Plateau composite section, warrant continued, focused paleontological study

6. CONCLUSIONS

We present new $\delta^{13}C_{carb\text{-}sh}$ and $\delta^{18}O_{carb\text{-}sh}$ data from carbonate cements within 107 shale samples of the terminal Ediacaran Nama Group, Namibia. These data are compared with the published $\delta^{13}C_{carb}$ and $\delta^{18}O_{carb}$ record derived from interbedded and laterally coeval carbonates throughout the Nama Group succession. Our preliminary results suggest that $\delta^{13}C_{carb\text{-}sh}$ recorded by samples deposited within mixed carbonate-clastic settings can approach $\delta^{13}C_{carb}$ if $CaCO_3$/TOC is sufficiently elevated. By contrast, shale samples with low $CaCO_3$/TOC deposited in clastic-only settings record values of $\delta^{13}C_{carb\text{-}sh}$ that are significantly depleted relative to $\delta^{13}C_{carb}$ in coeval carbonate-clastic successions. Intervals of the Nama Group succession characterized by both $\delta^{13}C$-$\delta^{18}O$ covariation and depleted $\delta^{13}C$ values appear to be restricted to those stratigraphic units and shallower facies that were more susceptible to mixing with meteoric fluids during early diagenesis. Recognition of these regional diagenetic effects permits a more accurate and detailed assessment of regional and global $\delta^{13}C_{carb}$ chemostratigraphy.

Despite these observations, the utility of $\delta^{13}C_{carb\text{-}sh}$ to infill gaps in the existing $\delta^{13}C_{carb}$ record remains unclear, even when using shale samples with high $CaCO_3$/TOC that were deposited in carbonate-clastic settings. For example, in the Nama Group, shale samples of the upper Schwarzrand Subgroup of the Witputs Sub-basin with elevated $CaCO_3$/TOC ratios record values of $\delta^{13}C_{carb\text{-}sh}$ that appear depleted relative to $\delta^{13}C_{carb}$ from underlying and overlying carbonate rocks. Robust comparison of trends in $\delta^{13}C_{carb\text{-}sh}$ and $\delta^{13}C_{carb}$ between sections in this interval is also impaired by the recognition of several possible lithostratigraphic correlations for key sections of the upper Schwarzrand Subgroup. Perhaps the most parsimonious lithostratigraphic alignment for this interval appears to support the synchronous development of carbonate pinnacle reefs in the Witputs and Vioolsdrif sub-basins of the Nama Group, associated with a major flooding (transgressive) event. This alignment may also result in temporal overlap of new $\delta^{13}C_{carb\text{-}sh}$ data in one section of the Witputs Sub-basin with a negative $\delta^{13}C_{carb}$ excursion that predates the 1n/BACE, and warrants future targeted paleontological, geochemical and stratigraphic study.

ACKNOWLEDGMENTS

We acknowledge funding from UKRI grant NE/T008458/1 and Beca de Doctorado en el Extranjero, Becas Chile from ANID. We thank C. Chilcott, G. Sim, H. Mocke, C. Hoffmann, A. and S. Horn, U. Schulze Neuhoff, C. Husselman, B. Romer and L. Gessert. We thank two anonymous reviewers, Chris Jones, Associate Editor Tim Lyons for thorough and thoughtful comments that helped to significantly improve this manuscript. For the purpose of open access, the authors have applied a Creative Commons Attribution (CC BY) license to any Author Accepted Manuscript version arising.

SUPPLEMENTARY INFORMATION

https://doi.org/10.17632/x2dnn8xcvy.1

Editor: C. Page Chamberlain, Mark Brandon, Associate Editor: Timothy W. Lyons

Submitted: January 18, 2022 EST, Accepted: August 15, 2023 EST

References

Ahm, A.-S. C., Bjerrum, C. J., Blättler, C. L., Swart, P. K., & Higgins, J. A. (2018). Quantifying early marine diagenesis in shallow-water carbonate sediments. *Geochimica et Cosmochimica Acta*, *236*, 140–159. https://doi.org/10.1016/j.gca.2018.02.042

Ahm, A.-S. C., Bjerrum, C. J., Hoffman, P. F., Macdonald, F. A., Maloof, A. C., Rose, C. V., Strauss, J. V., & Higgins, J. A. (2021). The Ca and Mg isotope record of the Cryogenian Trezona carbon isotope excursion. *Earth and Planetary Science Letters*, *568*, 117002. https://doi.org/10.1016/j.epsl.2021.117002

Ahm, A.-S. C., & Husson, J. (2022). *Local and Global Controls on Carbon Isotope Chemostratigraphy*. Cambridge University Press. https://doi.org/10.1017/9781009028882

Allan, J. R., & Matthews, R. K. (1982). Isotope signatures associated with early meteoric diagenesis. *Sedimentology*, *29*(6), 797–817. https://doi.org/10.1111/j.1365-3091.1982.tb00085.x

Blanco, G., Germs, G. J. B., Rajesh, H. M., Chemale, F., Jr., Dussin, I. A., & Justino, D. (2011). Provenance and paleogeography of the Nama Group (Ediacaran to early Palaeozoic, Namibia): Petrography, geochemistry and U-Pb detrital zircon geochronology. *Precambrian Research*, *187*(1–2), 15–32. https://doi.org/10.1016/j.precamres.2011.02.002

Blanco, G., Rajesh, H. M., Germs, G. J. B., & Zimmermann, U. (2009). Chemical composition and tectonic setting of chromian spinels from the Ediacaran-early Paleozoic Nama group, Namibia. *The Journal of Geology*, *117*(3), 325–341. https://doi.org/10.1086/597366

Boggiani, P. C., Gaucher, C., Sial, A. N., Babinski, M., Simon, C. M., Riccomini, C., Ferreira, V. P., & Fairchild, T. R. (2010). Chemostratigraphy of the Tamengo Formation (Corumbá Group, Brazil): A contribution to the calibration of the Ediacaran carbon-isotope curve. *Precambrian Research*, *182*(4), 382–401. https://doi.org/10.1016/j.precamres.2010.06.003

Bowring, S. A., Grotzinger, J. P., Condon, D. J., Ramezani, J., Newall, M. J., & Allen, P. A. (2007). Geochronologic constraints on the chronostratigraphic framework of the neoproterozoic Huqf Supergroup, Sultanate of Oman. *American Journal of Science*, *307*(10), 1097–1145. https://doi.org/10.2475/10.2007.01

Bowyer, F. T., Shore, A. J., Wood, R. A., Alcott, L. J., Thomas, A. L., Butler, I. B., Curtis, A., Hainanan, S., Curtis-Walcott, S., Penny, A. M., & Poulton, S. W. (2020). Regional nutrient decrease drove redox stabilisation and metazoan diversification in the late Ediacaran Nama Group, Namibia. *Scientific Reports*, *10*(1), 2240. https://doi.org/10.1038/s41598-020-59335-2

Bowyer, F. T., Uahengo, C.-I., Kaputuaza, K., Ndeunyema, J., Yilales, M., Alexander, R. D., Curtis, A., & Wood, R. A. (2023). Constraining the onset and environmental setting of metazoan biomineralization: the Ediacaran Nama Group of the Tsaus Mountains, Namibia. *Earth and Planetary Science Letters*, *620*, 118336. https://doi.org/10.1016/j.epsl.2023.118336

Bowyer, F. T., Zhuravlev, A. Y., Wood, R., Shields, G. A., Zhou, Y., Curtis, A., Poulton, S. W., Condon, D. J., Yang, C., & Zhu, M. (2022). Calibrating the temporal and spatial dynamics of the Ediacaran - Cambrian radiation of animals. *Earth-Science Reviews*, *225*, 103913. https://doi.org/10.1016/j.earscirev.2021.103913

Bowyer, F. T., Zhuravlev, A. Y., Wood, R., Zhao, F., Sukhov, S. S., Alexander, R. D., Poulton, S. W., & Zhu, M. (2023). Implications of an integrated late Ediacaran to early Cambrian stratigraphy of the Siberian Platform, Russia. *Geological Society of America Bulletin*. https://doi.org/10.1130/b36534.1

Brasier, M., Cowie, J., & Taylor, M. (1994). Decision on the Precambrian-Cambrian boundary stratotype. *Episodes*, *17*(1–2), 3–8. https://doi.org/10.18814/epiiugs/1994/v17i1.2/002

Canfield, D. E., Knoll, A. H., Poulton, S. W., Narbonne, G. M., & Dunning, G. R. (2020). Carbon isotopes in clastic rocks and the Neoproterozoic carbon cycle. *American Journal of Science*, *320*(2), 97–124. https://doi.org/10.2475/02.2020.01

Cochrane, D. J. W., Navarro, L., & Arnott, R. W. C. (2019). Sedimentological and geochemical evolution of an Ediacaran mixed carbonate-siliciclastic continental slope system, Windermere Supergroup, southern Canadian Cordillera, British Columbia, Canada. *Precambrian Research*, *327*, 47–67. https://doi.org/10.1016/j.precamres.2019.02.021

Cramer, B. D., & Jarvis, I. (2020). Carbon isotope stratigraphy. In F. M. Gradstein, J. G. Ogg, M. D. Schmitz, & G. M. Ogg (Eds.), *Geologic Time Scale 2020* (pp. 309–343). Elsevier B.V. https://doi.org/10.1016/b978-0-12-824360-2.00011-5

Cui, H., Warren, L. V., Uhlein, G. J., Okubo, J., Liu, X.-M., Plummer, R. E., Baele, J.-M., Goderis, S., Claeys, P., & Li, F. (2020). Global or regional? Constraining the origins of the middle Bambuí carbon cycle anomaly in Brazil. *Precambrian Research*, *348*, 105861. https://doi.org/10.1016/j.precamres.2020.105861

Darroch, S. A. F., Sperling, E. A., Boag, T. H., Racicot, R. A., Mason, S. J., Morgan, A. S., Tweedt, S., Myrow, P., Johnston, D. T., Erwin, D. H., & Laflamme, M. (2015). Biotic replacement and mass extinction of the Ediacara biota. *Proceedings of the Royal Society B: Biological Sciences*, *282*(1814), 20151003. https://doi.org/10.1098/rspb.2015.1003

Epstein, S., Buchsbaum, R., Lowenstam, H. A., & Urey, H. C. (1953). Revised carbonate-water isotopic temperature scale. *Geological Society of America Bulletin*, *64*(11), 1315–1326. https://doi.org/10.1130/0016-7606(1953)64[1315:RCITS]2.0.CO;2

Epstein, S., & Mayeda, T. (1953). Variation of O18 content of waters from natural sources. *Geochimica et Cosmochimica Acta*, *4*(5), 213–224. https://doi.org/10.1016/0016-7037(53)90051-9

Germs, G. J. B. (1974). The Nama Group in South West Africa and Its Relationship to the Pan-African Geosyncline. *The Journal of Geology*, *82*(3), 301–317. https://doi.org/10.1086/627966

Germs, G. J. B. (1983). Implications of a sedimentary facies and depositional environmental analysis of the Nama Group in South West Africa/Namibia. *Special Publications of the Geological Society of South Africa*, *11*, 89–114.

Germs, G. J. B., & Gresse, P. G. (1991). The foreland basin of the Damara and Gariep orogens in Namaqualand and southern Namibia: stratigraphic correlations and basin dynamics. *South African Journal of Geology*, *94*(2), 159–169.

Geyman, E. C., & Maloof, A. C. (2019). A diurnal carbon engine explains ^{13}C-enriched carbonates without increasing the global production of oxygen. *Proceedings of the National Academy of Sciences of the United States of America*, *116*(49), 24433–24439. https://doi.org/10.1073/pnas.1908783116

Gresse, P. G., & Germs, G. J. B. (1993). The Nama foreland basin: sedimentation, major unconformity bounded sequences and multisided active margin advance. *Precambrian Research*, *63*(3–4), 247–272. https://doi.org/10.1016/0301-9268(93)90036-2

Grotzinger, J. P., Bowring, S. A., Saylor, B. Z., & Kaufman, A. J. (1995). Biostratigraphic and geochronological constraints on early animal evolution. *Science*, *270*(5236), 598–604. https://doi.org/10.1126/science.270.5236.598

Halverson, G. P., Hoffman, P. F., Schrag, D. P., Maloof, A. C., & Rice, A. H. N. (2005). Toward a Neoproterozoic composite carbon-isotope record. *Geological Society of America Bulletin*, *117*(9), 1181–1207. https://doi.org/10.1130/b25630.1

Hodgin, E. B., Nelson, L. L., Wall, C. J., Barrón-Díaz, A. J., Webb, L. C., Schmitz, M. D., Fike, D. A., Hagadorn, J. W., & Smith, E. F. (2021). A link between rift-related volcanism and end-Ediacaran extinction? Integrated chemostratigraphy, biostratigraphy, and U-Pb geochronology from Sonora, Mexico. *Geology*, *49*(2), 115–119. https://doi.org/10.1130/g47972.1

Hoffman, P. F., & Lamothe, K. G. (2019). Seawater-buffered diagenesis, destruction of carbon isotope excursions, and the composition of DIC in Neoproterozoic oceans. *Proceedings of the National Academy of Sciences of the United States of America*, *116*(38), 18874–18879. https://doi.org/10.1073/pnas.1909570116

Jensen, S., Saylor, B. Z., Gehling, J. G., & Germs, G. J. B. (2000). Complex trace fossils from the terminal Proterozoic of Namibia. *Geology*, *28*(2), 143–146.

Khadka, M. B., Martin, J. B., & Jin, J. (2014). Transport of dissolved carbon and CO2 degassing from a river system in a mixed silicate and carbonate catchment. *Journal of Hydrology*, *513*, 391–402. https://doi.org/10.1016/j.jhydrol.2014.03.070

Kouchinsky, A., Bengtson, S., Pavlov, V., Runnegar, B., Torssander, P., Young, E., & Ziegler, K. (2007). Carbon isotope stratigraphy of the Precambrian-Cambrian Sukharikha River section, northwestern Siberian platform. *Geological Magazine*, *144*(4), 609–618. https://doi.org/10.1017/s0016756807003354

Linnemann, U., Ovtcharova, M., Schaltegger, U., Gärtner, A., Hautmann, M., Geyer, G., Vickers-Rich, P., Rich, T., Plessen, B., Hofmann, M., Zieger, J., Krause, R., Kriesfeld, L., & Smith, J. (2019). New high-resolution age data from the Ediacaran-Cambrian boundary indicate rapid, ecologically driven onset of the Cambrian explosion. *Terra Nova*, *31*(1), 49–58. https://doi.org/10.1111/ter.12368

Maloney, K. M., Boag, T. H., Facciol, A. J., Gibson, B. M., Cribb, A., Koester, B. E., Kenchington, C. G., Racicot, R. A., Darroch, S. A. F., & Laflamme, M. (2020). Paleoenvironmental analysis of Ernietta-bearing Ediacaran deposits in southern Namibia. *Palaeogeography, Palaeoclimatology, Palaeoecology*, *556*, 109884. https://doi.org/10.1016/j.palaeo.2020.109884

Maloof, A. C., Porter, S. M., Moore, J. L., Dudás, F. Ö., Bowring, S. A., Higgins, J. A., Fike, D. A., & Eddy, M. P. (2010). The earliest Cambrian record of animals and ocean geochemical change. *Geological Society of America Bulletin*, *122*(11–12), 1731–1774. https://doi.org/10.1130/b30346.1

Melim, L. A., Westphal, H., Swart, P. K., Eberli, G. P., & Munnecke, A. (2002). Questioning carbonate diagenetic paradigms: Evidence from the Neogene of the Bahamas. *Marine Geology*, *185*(1–2), 27–53. https://doi.org/10.1016/s0025-3227(01)00289-4

Messori, F., Ovtcharova, M., Zieger, J., Geyer, G., Linnemann, U., Hofmann, M., & Vickers-Rich, P. (2021). New high precision U-Pb CA-ID-TIMS zircon ages from the Terminal Ediacaran in Namibia. *Goldschmidt, July 2021 Abstracts with Programs*. https://doi.org/10.7185/gold2021.7132

Nelson, L. L., Crowley, J. L., Smith, E. F., Schwartz, D. M., Hodgin, E. B., & Schmitz, M. D. (2023). Cambrian explosion condensed: High-precision geochronology of the lower Wood Canyon Formation, Nevada. *Proceedings of the National Academy of Sciences of the United States of America*, *120*(30), e2301478120. https://doi.org/10.1073/pnas.2301478120

Nelson, L. L., Ramezani, J., Almond, J. E., Darroch, S. A. F., Taylor, W. L., Brenner, D. C., Furey, R. P., Turner, M., & Smith, E. F. (2022). Pushing the boundary: A calibrated Ediacaran-Cambrian stratigraphic record from the Nama Group in northwestern Republic of South Africa. *Earth and Planetary Science Letters*, *580*, 117396. https://doi.org/10.1016/j.epsl.2022.117396

Parry, L. A., Boggiani, P. C., Condon, D. J., Garwood, R. J., Leme, J. de M., McIlroy, D., Brasier, M. D., Trindade, R., Campanha, G. A. C., Pacheco, M. L. A. F., Diniz, C. Q. C., & Liu, A. G. (2017). Ichnological evidence for meiofaunal bilaterians from the terminal Ediacaran and earliest Cambrian of Brazil. *Nature Ecology & Evolution*, *1*(10), 1455–1464. https://doi.org/10.1038/s41559-017-0301-9

Pelechaty, S. M., Kaufman, A. J., & Grotzinger, J. P. (1996). Evaluation of δ13C chemostratigraphy for intrabasinal correlation: Vendian strata of northeast Siberia. *Geological Society of America Bulletin*, *108*(8), 992–1003.

Rodriguez Blanco, L., Eberli, G. P., Weger, R. J., Swart, P. K., Tenaglia, M., Rueda Sanchez, L. E., & McNeill, D. F. (2020). Periplatform ooze in a mixed siliciclastic-carbonate system - Vaca Muerta Formation, Argentina. *Sedimentary Geology*, *396*, 105521. https://doi.org/10.1016/j.sedgeo.2019.105521

Rogov, V. I., Karlova, G. A., Marusin, V. V., Kochnev, B. B., Nagovitsin, K. E., & Grazhdankin, D. V. (2015). Duration of the first biozone in the Siberian hypostratotype of the Vendian. *Russian Geology and Geophysics*, *56*(4), 573–583. https://doi.org/10.1016/j.rgg.2015.03.016

Rooney, A. D., Cantine, M. D., Bergmann, K. D., Gómez-Pérez, I., Al Baloushi, B., Boag, T. H., Busch, J. F., Sperling, E. A., & Strauss, J. V. (2020). Calibrating the coevolution of Ediacaran life and environment. *Proceedings of the National Academy of Sciences of the United States of America*, *117*(29), 16824–16830. https://doi.org/10.1073/pnas.2002918117

Saltzman, M. R., & Thomas, E. (2012). Carbon Isotope Stratigraphy. In F. M. Gradstein, J. G. Ogg, M. D. Schmitz, & G. M. Ogg (Eds.), *The Geological Time Scale 2012* (pp. 207–232). Elsevier B.V. https://doi.org/10.1016/b978-0-444-59425-9.00011-1

Saylor, B. Z. (2003). Sequence stratigraphy and carbonate-siliciclastic mixing in a terminal Proterozoic foreland basin, Urusis Formation, Nama Group, Namibia. *Journal of Sedimentary Research*, *73*(2), 264–279. https://doi.org/10.1306/082602730264

Saylor, B. Z., & Grotzinger, J. P. (1996). Reconstruction of important Proterozoic-Cambrian boundary exposures through the recognition of thrust deformation in the Nama Group of southern Namibia. *Communications of the Geological Survey of Namibia*, *11*, 1–12.

Saylor, B. Z., Grotzinger, J. P., & Germs, G. J. B. (1995). Sequence stratigraphy and sedimentology of the Neoproterozoic Kuibis and Schwarzrand Subgroups (Nama Group), southwestern Namibia. *Precambrian Research*, *73*(1–4), 153–171. https://doi.org/10.1016/0301-9268(94)00076-4

Saylor, B. Z., Kaufman, A. J., Grotzinger, J. P., & Urban, F. (1998). A composite reference section for terminal Proterozoic strata of southern Namibia. *Journal of Sedimentary Research*, *68*(6), 1223–1235. https://doi.org/10.2110/jsr.68.1223

Schmitz, M. D. (2012). Radiogenic Isotope Geochronology. In F. M. Gradstein, J. G. Ogg, M. D. Schmitz, & G. M. Ogg (Eds.), *The Geological Time Scale 2012* (pp. 115–126). Elsevier. https://doi.org/10.1016/b978-0-444-59425-9.00006-8

Selly, T., Schiffbauer, J. D., Jacquet, S. M., Smith, E. F., Nelson, L. L., Andreasen, B. D., Huntley, J. W., Strange, M. A., O'Neil, G. R., Thater, C. A., Bykova, N., Steiner, M., Yang, B., & Cai, Y. (2020). A new cloudinid fossil assemblage from the terminal Ediacaran of Nevada, USA. *Journal of Systematic Palaeontology*, *18*(4), 357–379. https://doi.org/10.1080/14772019.2019.1623333

Smith, E. F., Macdonald, F. A., Petach, T. A., Bold, U., & Schrag, D. P. (2016). Integrated stratigraphic, geochemical, and paleontological late Ediacaran to early Cambrian records from southwestern Mongolia. *Geological Society of America Bulletin*, *128*(5–6), 1056–1056. https://doi.org/10.1130/b31248.1

Smith, E. F., Nelson, L. L., Strange, M. A., Eyster, A. E., Rowland, S. M., Schrag, D. P., & Macdonald, F. A. (2016). The end of the Ediacaran: Two new exceptionally preserved body fossil assemblages from Mount Dunfee, Nevada, USA. *Geology*, *44*(11), 911–914. https://doi.org/10.1130/g38157.1

Smith, O. (1999). *Terminal Proterozoic carbonate platform development: stratigraphy and sedimentology of the Kuibis Subgroup (ca. 550–548 Ma), northern Nama Basin, Namibia* [Unpublished Masters dissertation, Massachusetts Institute of Technology]. http://hdl.handle.net/1721.1/36672

Swart, P. K. (2015). The geochemistry of carbonate diagenesis: The past, present and future. *Sedimentology*, *62*(5), 1233–1304. https://doi.org/10.1111/sed.12205

Tarutani, T., Clayton, R. N., & Mayeda, T. K. (1969). The effect of polymorphism and magnesium substitution on oxygen isotope fractionation between calcium carbonate and water. *Geochimica et Cosmochimica Acta*, *33*(8), 987–996. https://doi.org/10.1016/0016-7037(69)90108-2

Topper, T., Betts, M. J., Dorjnamjaa, D., Li, G., Li, L., Altanshagai, G., Enkhbaatar, B., & Skovsted, C. B. (2022). Locating the BACE of the Cambrian: Bayan Gol in southwestern Mongolia and global correlation of the Ediacaran-Cambrian boundary. *Earth-Science Reviews*, *229*, 104017. https://doi.org/10.1016/j.earscirev.2022.104017

Urey, H. C. (1947). The thermodynamic properties of isotopic substances. *Journal of the Chemical Society (Resumed)*, 562–581. https://doi.org/10.1039/jr9470000562

Veizer, J., & Hoefs, J. (1976). The nature of O18/O16 and C13/C12 secular trends in sedimentary carbonate rocks. *Geochimica et Cosmochimica Acta*, *40*(11), 1387–1395.

Wood, R. A., Bowyer, F., Penny, A., & Poulton, S. W. (2018). Did anoxia terminate Ediacaran benthic communities? Evidence from early diagenesis. *Precambrian Research*, *313*, 134–147. https://doi.org/10.1016/j.precamres.2018.05.011

Wood, R. A., Poulton, S. W., Prave, A. R., Hoffmann, K.-H., Clarkson, M. O., Guilbaud, R., Lyne, J. W., Tostevin, R., Bowyer, F., Penny, A. M., Curtis, A., & Kasemann, S. A. (2015). Dynamic redox conditions control late Ediacaran metazoan ecosystems in the Nama Group, Namibia. *Precambrian Research*, *261*, 252–271. https://doi.org/10.1016/j.precamres.2015.02.004

Yang, C., Rooney, A. D., Condon, D. J., Li, X.-H., Grazhdankin, D. V., Bowyer, F. T., Hu, C., Macdonald, F. A., & Zhu, M. (2021). The tempo of Ediacaran evolution. *Science Advances*, *7*(45), eabi9643. https://doi.org/10.1126/sciadv.abi9643

Zhu, M.-Y., Babcock, L. E., & Peng, S.-C. (2006). Advances in Cambrian stratigraphy and paleontology: Integrating correlation techniques, paleobiology, taphonomy and paleoenvironmental reconstruction. *Palaeoworld*, *15*(3–4), 217–222. https://doi.org/10.1016/j.palwor.2006.10.016

Zhu, M.-Y., Yang, A., Yuan, J., Li, G., Zhang, J., Zhao, F., Ahn, S.-Y., & Miao, L. (2019). Cambrian integrative stratigraphy and timescale of China. *Science China Earth Sciences*, *62*(1), 25–60. https://doi.org/10.1007/s11430-017-9291-0

Supplementary Materials

SUPPLEMENTARY INFORMATION for: 'Insights into the terminal Ediacaran marine carbonate record from shale-hosted carbonate carbon isotopes'

Download: https://ajsonline.org/article/88082-insights-into-the-terminal-ediacaran-marine-carbonate-record-from-shale-hosted-carbonate-carbon-isotopes/attachment/181309.docx